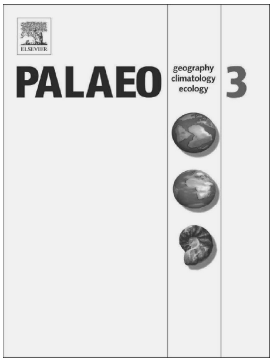

Taphonomy and palaeoecology of the lower Miocene marine vertebrate assemblage of Ullujaya (Chilcatay Formation, East Pisco Basin, southern Peru)

Giovanni Bianucci, Alberto Collareta, Giulia Bosio, Walter Landini, Karen Gariboldi, Anna Gioncada, Olivier Lambert, Elisa Malinverno, Christian de Muizon, Rafael Varas-Malca, Igor Maria Villa, Giovanni Coletti, Mario Urbina, Claudio Di Celma

PII: S0031-0182(18)30483-8
DOI: doi:10.1016/j.palaeo.2018.08.013
Reference: PALAEO 8899

To appear in: *Palaeogeography, Palaeoclimatology, Palaeoecology*

Received date: 28 May 2018
Revised date: 20 August 2018
Accepted date: 21 August 2018

Please cite this article as: Giovanni Bianucci, Alberto Collareta, Giulia Bosio, Walter Landini, Karen Gariboldi, Anna Gioncada, Olivier Lambert, Elisa Malinverno, Christian de Muizon, Rafael Varas-Malca, Igor Maria Villa, Giovanni Coletti, Mario Urbina, Claudio Di Celma , Taphonomy and palaeoecology of the lower Miocene marine vertebrate assemblage of Ullujaya (Chilcatay Formation, East Pisco Basin, southern Peru). Palaeo (2018), doi:10.1016/j.palaeo.2018.08.013

Taphonomy and palaeoecology of the lower Miocene marine vertebrate assemblage of Ullujaya (Chilcatay Formation, East Pisco Basin, southern Peru)

Giovanni Bianucci[1,*], Alberto Collareta[1], Giulia Bosio[2], Walter Landini[1], Karen Gariboldi[1], Anna Gioncada[1], Olivier Lambert[3], Elisa Malinverno[2], Christian de Muizon[4], Rafael Varas-Malca[5], Igor Maria Villa[2], Giovanni Coletti[2], Mario Urbina[5], Claudio Di Celma[6]

[1] Dipartimento di Scienze della Terra, Università di Pisa, 56126 Pisa, Italy

[2] Dipartimento di Scienze dell'Ambiente e della Terra, Università di Milano Bicocca, 20126 Milano, Italy

[3] D.O. Terre et Histoire de la Vie, Institut Royal des Sciences Naturelles de Belgique, 1000 Brussels, Belgium

[4] Département Origines et Évolution, Muséum National d'Histoire Naturelle, Centre de Recherches sur la paléobiodiversité et les paléoenvironnements – CR2P (CNRS, MNHN, Sorbonne Université), 75005 Paris, France

[5] Departamento de Paleontologia de Vertebrados, Museo de Historia Natural de la Universidad Nacional Mayor de San Marcos, avenida Arenales 1256, Lima 14, Peru

[6] Scuola di Scienze e Tecnologie, Università di Camerino, 62032 Camerino, Italy

** Corresponding author. E-mail address: bianucci@dst.unipi.it*

Abstract

The taphonomy and palaeoecology of the early Miocene (Burdigalian) vertebrate assemblage of Ullujaya (East Pisco Basin, Peru) is here described. Vertebrate remains are concentrated in marine facies (*Ct1a* association) of the exposed Chilcatay Formation (dated 19-18 Ma) deposited within a 30-40 m deep, semi-enclosed, offshore environment. Coupled with ichnological observations, the size distribution of pyrite framboid relics reveals fluctuation of euxinic and oxic-dysoxic conditions at the seafloor. The assemblage is dominated by toothed cetaceans (kentriodontids, squalodelphinids, physeteroids, and the eurhinodelphinid-like *Chilcacetus*), together with a large dermochelyid turtle, some bony fish, and diverse elasmobranchs, mostly juveniles of *Carcharhinus brachyurus* and *Cosmopolitodus hastalis*. The vertebrate assemblage comprises a coastal community, dominated by mesopredators, representative of a warm-temperate, sheltered embayment connected with riverine and open-ocean environments. Vertebrate skeletons are typically disarticulated and incomplete, and some bone elements display shark bite marks. Microborings are observed at the bone surface. Bones exhibit a good degree of apatite mineralisation and bone cavities are locally filled by Ca-Mg carbonates. Our taphonomic observations suggest prolonged flotation of carcasses during which they were subject to biogenic and physical processes of partial destruction (including scavenging by sharks), before final deposition on a soft compact substrate. Preservation was favoured by the oxygen-deficient bottom conditions that inhibited the action of benthic macro-scavengers.

Keywords

Burdigalian, Cetacea, Elasmobranchii, Fossil-Lagerstätte, palaeoenvironments, taphonomy.

1. Introduction

Remarkable global climatic, oceanographic, and seal-level changes occurred during the

Cenozoic, promoting the redistribution and partitioning of food resources and consequent changes in diversity and disparity of marine vertebrates (Norris et al., 2013). Although some general models linking these environmental changes to the evolution of different marine vertebrate lineages have already been proposed (Marx and Uhen 2010), our knowledge of Cenozoic marine vertebrates is still primarily based on a chronostratigraphically and geographically heterogeneous fossil record. For these reasons, the reliability of such models in depicting global evolutionary trends has been questioned (Pyenson et al., 2010).

Contrasting with this fragmentary global scenario, the Eocene to Pliocene fill of the East Pisco Basin, southern coast of Peru (hereinafter: EPB), features one of the largest concentrations of Cenozoic marine vertebrate fossils discovered worldwide. The fossil content of the (?)middle Miocene to Pliocene Pisco Formation, the youngest portion of the basin fill, is well-known from a systematic, palaeoecological and taphonomic point of view, based on thirty-five years of research efforts (see Bianucci et al. 2016a, b and Di Celma et al. 2017 for a complete reference list). Besides strongly contributing to the clarification of several aspects of the Neogene global evolutionary trends for several marine vertebrate lineages, these studies also provided insights into the genesis of the extraordinary fossil assemblage of the Pisco Formation. By contrast, the knowledge on the fossil contents of the older deposits of the EPB is still fragmentary, although including some specimens of extraordinary relevance, for both their evolutionary significance and their exceptional preservation (e.g., Clarke et al, 2010; Uhen et al., 2011; Lambert et al. 2017a; Martínez-Cáceres et al., 2017). Moreover, studies carried out in the last years by our team highlighted an unexpected abundance of fossil vertebrates in the lower Miocene strata of the Chilcatay Formation.

All fossil vertebrates represented by bone elements described so far from this formation belong to odontocetes (toothed whales) and particularly to the platanistoid family Squalodelphinidae (Lambert et al. 2014; Bianucci et al., 2015, 2018), the new family Inticetidae (Lambert et al., 2018), and the longirostrine eurhinodelphid-like genus *Chilcacetus* (Lambert et al., 2015b). In addition, the

fossil assemblages of some shark tooth-rich beds have been described in detail (Landini et al., 2018).

Most of these fossils have been discovered in a few localities along the western side of the Ica River (e.g., Roca Negra, Ullujaya, and Zamaca), where the Chilcatay beds are extensively exposed. The aim of the present interdisciplinary work is to describe the marine vertebrate assemblage of one of these localities – Ullujaya – from a taphonomic and palaeoecological point of view in order to define the conditions and processes leading to the preservation of such a remarkable fossil record and to assess the ecological significance of this assemblage in the global evolutionary scenario of the Miocene marine vertebrate biota.

2. Tectono-stratigraphic context

Since Mesozoic times, the tectono-dynamics of Peru have been controlled by the convergence of the oceanic Nazca/Farallon Plate and the continental South American Plate. This transform-convergent margin, characterised by normal to strike-slip faults, formed elongated basins along the Peruvian forearc (Kulm et al., 1982; Dunbar et al., 1990; León et al., 2008; Zúñiga-Rivero et al., 2010; Viveen and Schlunegger, 2018) (Fig. 1). According to Thornburg and Kulm (1981), two long and narrow, trench-parallel structural highs - the Outer Shelf High and the Upper Slope Ridge - formed on the continental shelf and upper slope in Late Cretaceous–early Palaeogene times, segmenting the Peruvian offshore into an inner set of shelf basins and a seaward set of slope basins (Fig. 1A). In this frame, the onshore EPB lies east of the Outer Shelf High as a shelf basin, whereas the still-submerged West Pisco Basin lies west of the Outer Shelf High as an upper-slope basin. Active subduction erosion (von Huene and Lallemand, 1990; Clift et al., 2003; Hampel et al., 2004) controlled a prolonged period of normal faulting and subsidence in the EPB since at least the middle-late Eocene (Dunbar et al., 1990; León et al., 2008; Rustichelli et al., 2016a, b). This protracted extensional regime was only interrupted during the middle Miocene by a widespread

pulse of uplift, possibly related to the Quechua 1 tectonic event (Viveen and Schlunegger, 2018).

The sedimentary fill of the EPB comprises, from the oldest to the youngest, the Eocene Caballas Formation and Paracas Group (including the Los Choros and Yumaque formations), the upper Oligocene–middle Miocene Chilcatay Formation, and the (?)middle Miocene–Pliocene Pisco Formation (Dunbar et al., 1990; DeVries, 1998, 2017; DeVries et al., 2017; DeVries and Jud, 2018). Some of these units are bounded by regionally extensive angular unconformities, which account for periods of subaerial exposure (DeVries, 1998). During deposition of the Chilcatay Formation, the EPB was a shallow-water, semi-enclosed embayment bounded to the east by the Coastal Batholith (a complex of igneous rocks mostly emplaced during the Late Cretaceous–early Eocene) and protected to the west by a chain of crystalline basement islands (Marocco and Muizon, 1988; the Gran Tablazo Archipelago of DeVries and Jud, 2018) (Fig. 1B).

3. Study area and methods

Ullujaya is a richly fossiliferous site located in the Ocucaje area, along the western side of the Ica River, in the southern coastal desert of Peru (Fig. 1C). In this area, the Chilcatay Formation comprises two smaller units (namely, the Ct1 and Ct2 allomembers), separated by a major intraformational unconformity, CE0.2 (Figs. 2 and 3A). The stratigraphic interval of interest for the present study comprises the middle to upper part of the Ct1 allomember, since the older Ct1 strata and the unconformity at the base of the formation (CE0.1) are not exposed at Ullujaya. By using a 66-m-long measured section and a high-resolution geological map (Fig. 2), the vertebrate fossil assemblages of the Chilcatay Formation exposed in this area have already been placed into a proper sedimentological, stratigraphic, and chronostratigraphic context by Di Celma et al. (2018).

Twenty-three sediment samples were collected along the measured section for palaeoecological, sedimentological, and chronostratigraphic purposes. Smear slides of fine-grained sediments were analysed with an Olympus BX50 polarised optical microscope. Diatoms and silicoflagellates were

analysed at 1000x. Some samples were analysed using a ZEISS Scanning Electron Microscope, after carbon coating. The size distribution of relics of pyrite framboids was used as an indicator of redox conditions (Wilkin et al., 1996). For the chronostratigraphic study, biotite phenocrysts from a tephra deposit were analysed for major elements using a JEOL 8200 Super Probe at the University of Milan to check for alteration. $^{40}Ar/^{39}Ar$ analyses were performed on hand-picked biotite crystals at the University of Milano-Bicocca, with the NuInstruments™ Noblesse® noble gas mass spectrometer, using an updated procedure based on Villa et al. (2000). The sample was irradiated avoiding Cd shielding in the nuclear reactor at the McMaster University (Canada); the Fish Canyon sanidine was used as flux monitor (assumed age: 28.172 ± 0.028 Ma, Rivera et al., 2011).

Macroscopic taphonomic data were collected both in the field and at the Museo de Historia Natural de la Universidad Nacional Mayor de San Marcos (hereinafter: MUSM) by examining fossils collected over the past years from the Ullujaya locality. Field observations were limited by the fact that most of the exposed specimens are still included in partially lithified sediment that has not been removed to avoid damaging the bones. Moreover, recent erosion partially destroyed and/or displaced the exposed bones. For selecting, describing, and quantifying this taphonomic information we also considered previous studies about the taphonomy of fossil vertebrates, with particular attention to the few papers dealing with marine mammal assemblages (e.g., Boessenecker et al., 2014, Danise and Dominici, 2014; Esperante et al. 2015). The articulation degree of associated bones was coded with numbers from 4 to 1 as follows: 4 (100-75% bones articulated); 3 (75-50%); 2 (50-25%); 1 (>25%); 0 (fully disarticulated bones). Similarly, for skeletal completeness: 4 (100-75% of the skeleton preserved); 3 (75-50%); 2 (50-25%); 1 (< 25%); 0 (one bone or one skeletal element, e.g. the cranium, preserved). Articulation and completeness of the cetacean skeletons were also quantitatively evaluated by using an approach similar to that used by Beardmore et al. (2012) and Beardmore and Furrer (2016a,b) for marine reptiles. Degrees of articulation and completeness, expressed as percentages, were plotted on a bivariate bubble plot in Microsoft Excel. A best-fit

linear trend line, forced through the point corresponding to 100% completeness and 100% articulation (i.e., the 'taphonomic origin' of the data, reflecting the common condition of specimens at death), was obtained. The 'T-value' was then defined by the intersect of the aforementioned trend line with the completeness axis. Pearson's r^2 value, indicating the goodness of fit of the regression line, was also obtained with Excel. Finally, the Spearman rank-order correlation coefficient (rs) was calculated in PAST (PAlaeontological STatistics program; Hammer and Harper, 2001) for having a non-parametric measure of the strength of correlation between articulation and completeness. Given the significant differences between reptile and cetacean skeletons (e.g., the cranial bones of cetaceans are less subject to disarticulation than those of reptiles), and considering also the relatively small size of our dataset (we analysed 52 specimens, excluding the remains exhibiting significant recent erosion and/or skeletons not found *in situ*), differing from Beardmore et al. (2012) and Beardmore and Furrer (2016a,b), we did not divide the skeleton in distinct units for the purposes of the quantitative taphonomic analysis.

In the field, taphonomic observations concerned the degree of preservation of the cortical bone and vertebral processes, as well as the presence/absence of: 1) bone abrasion; 2) bone fractures; 3) associated mollusc shells, remains of crabs and other invertebrates, teleostean and elasmobranch teeth; 4) associated remains of encrusting epibionts; and 5) traces of invertebrates and vertebrates.

Shark bite marks were analysed using the morphological-genetic approach proposed by Cigala Fulgosi (1990) and modified by Bianucci et al. (2010b) and Collareta et al. (2017a), distinguishing five types of bite marks (Type I to V) on the basis of the producing impact.

For microscopic taphonomic features, nine bone samples from seven cetacean specimens were prepared as polished thin sections cut orthogonally to the elongation of the bone. They were analysed with Olympus BX50 and Leica Leitz Laborlux S transmitted light and Leica DM EP reflected light microscopes and with scanning electron microscopy and microanalysis (SEM-EDS; Tescan VEGA TS 5136 XM, University of Milano-Bicocca and the Philips -EDAX Genesis

University of Pisa), obtaining semi-quantitative composition results.

4. Results

4.1. Stratigraphy, sedimentology, and age of the Chilcatay Formation at Ullujaya

The exposed portion of the Ct1 allomember is about 56 m thick and comprises a distinct two-fold subdivision of sedimentary facies, which includes a sub-horizontal package of interbedded medium- to fine-grained sandstones, sandy siltstones and siltstones (*Ct1a* facies association) and a stack of clinoformed units having a mixed siliciclastic-carbonate composition (*Ct1b* facies association).

The bulk of *Ct1a* is characterised by the dominance of massive, medium- to fine-grained siliciclastic sandstones and siltstones (Fig. 3B) with rare occurrences of silicoflagellates and diatoms, dominated by genera that are typical of coastal settings (*Actinoptychus*, *Cocconeis*, *Delphineis*, *Grammatophora*, *Paralia*). The diluted coarse biogenic fraction is composed of small amounts of redeposited skeletal elements including barnacles and mollusc shells (mainly ostreids and pectinids), both occurring as fragments and complete specimens, and rare echinoids and calcareous worm tubes. Rare encrusting bryozoans were observed on barnacle shells.

These fine-grained sediments are punctuated by laterally persistent beds of granule- to coarse-grained sandstones that range from 0.1 to 0.5 m in thickness and, locally, pass laterally into erosionally based cobble- to boulder-sized conglomerates up to 1.5 m thick. The bases of the granule- to coarse-grained sandstone beds are sharp and display dense burrow assemblages dominated by large *Thalassinoides* and subordinate *Gyrolithes* penetrating deeply into the subjacent fine-grained sediments (Figs. 3C, D). The burrows are backfilled with sediment from the overlying coarse-grained bed. The composition of the granule layers is a laterally variable mixture of siliciclastic grains, broken or whole shells of barnacles and small molluscs fragments, whereas that of the cobble- to boulder-sized conglomerates is dominated by rounded clasts from volcanic ash

tuffs and from the igneous basement set in a coarse-grained bioclastic matrix.

During microscopic observations, abundant, subspherical framboidal aggregates of Fe-oxyhydroxide microcrystals, representing relic textures of pyrite framboids were detected through the sediment, which consists of small rhombohedral crystals of dolomite terrigenous clasts, and biogenic fragments (Fig. 4). The diameter of the framboids was measured in five samples from *Ct1a*, selected between 22 and 28.5 m above the base of the measured section (abbreviated: abs), where a high concentration of fossil vertebrates was found (Fig. 5). Framboids from 22 m abs, 23.5 m abs, 26 m abs, and 28.5 m abs exhibit a mean diameter of 4.6 ± 2.0 μm (as 1σ), 5.1 ± 1.9 μm, 5.3 ± 2.2 μm, and 5.0 ± 1.9 μm, respectively. Sample UL-D3 (25 m abs) exhibits a higher mean diameter of 8.3 ± 4.8 μm. Framboids having a diameter greater than 10 μm are 3.8% at most except for sample UL-D3 having a high percentage of large framboids (32.5%). Irregularly-shaped framboids are rare and concentrated in sample UL-D3.

Sediments of *Ct1a* underlie and, locally, landward interfinger with a 20-m-thick, clinostratified carbonate wedge (*Ct1b*). The dip direction of clinobeds is dominantly oriented to the southwest, indicating a uniform progradation direction. Clinoform height attains 15-20 m and maximum declivity ranges between 15° and 20°. Individual clinobeds are between 0.2 and 0.5 m thick and are composed of coarse-grained, well-sorted, skeletal-rich grainstones mixed with subordinate amounts of granule- and small pebble-sized terrigenous components. In terms of skeletal composition, *Ct1b* is largely dominated by large-sized, hard-substrate-related shore barnacles, occurring either as fragmented individuals or as clusters, with lesser amounts of molluscs, benthic foraminifera, and echinoids, representing a typical heterozoan assemblage (*sensu* James, 1997). All shells exhibit a high degree of fragmentation and disarticulation, and variably abraded shapes, indicative of transport. The lower boundary of the clinobedded deposit is a downlap surface characterised by a sharp and undulated lithologic contact with underlying sediments of *Ct1a*.

Diatom and silicoflagellate biostratigraphy already provides a robust chronology for the strata

exposed at Ullujaya and allows to define an age comprised between 18 and 19 Ma, with the age of the youngest portion of the section being in agreement with the $^{40}Ar/^{39}Ar$ age of 18.02 ± 0.07 Ma obtained from biotite in tephra SOT-T3, sampled just 1 m below the erosional contact with the overlying Pisco Formation (Di Celma et al., 2018). This chronostratigraphic framework is here further supported by a new $^{40}Ar/^{39}Ar$ dating of a volcanic ash layer (UJA-T35) sampled 2 m above the lowermost exposure of the Ct1 allomember at Ullujaya.

Although microprobe analyses on biotite phenocrysts from this ash layer highlighted a loss of K in the interlayer occupancy, it was one of the best preserved among the very few tephra detectable in the section. The isochemical steps probably circumvent the alteration and give a $^{40}Ar/^{39}Ar$ age of 19.00 ± 0.28 Ma (2σ uncertainty).

4.2. Overall composition of the fossil vertebrate assemblage

The assemblage includes bony vertebrates and chondrichthyan teeth. Eighty-two marine vertebrate specimens are preserved as bony elements (Table 1). Remains of Cetacea dominate this assemblage, accounting for 86.6% of the specimens, with a large number of indeterminate specimens (56.1%). All specimens identifiable to suborder level belong to Odontoceti and no baleen whale (Mysticeti) is recorded so far. Odontocete remains belong to Kentriodontidae (19.6%; early relatives of today's true dolphins and porpoises), Squalodelphinidae (6.1%; a family closely related to the extant South Asian river dolphin), Physeteroidea (2.4%; sperm whales), and to the genus *Chilcacetus* (2.4%; an extinct lineage of homodont, long-snouted dolphins) (Fig. 6B). Kentriodontids belong to an undescribed species within the genus *Kentriodon* Kellogg, 1927. This kentriodontid is the most common cetacean taxon at Ullujaya, being known by several crania, some of which are associated with mandibles and partial postcranial. Seven of these crania (MUSM 586, 631, 1393, 1397, 1398, and 2431) have been collected and are now under study. Squalodelphinid remains include: 1) two specimens of *Huaridelphis raimondii* (the holotype MUSM 1396,

consisting of an isolated cranium, and the referred specimen MUSM 1403, a cranium, fragmentary mandible and some associated postcranial bones) (Lambert et al., 2014); 2) a well-preserved specimen attributed to *Notocetus vanbenedeni* (MUSM 1395, consisting of a cranium with an associated cervical vertebra) (Bianucci et al., 2015); and 3) two indeterminate specimens consisting of a disarticulated partial skeleton (MUSM 1484) and an isolated tympanic bulla (MUSM 1485). Physeteroids consist of two isolated crania: 1) MUSM 3246, referred to cf. *Diaphorocetus* sp., sharing some affinities with *Diaphorocetus poucheti* from the lower Miocene Monte León Formation of Argentina; and 2) one badly damaged specimen previously regarded as an indeterminate mysticete (Lambert et al., 2014, Bianucci et al., 2015) but now confidently identified as a sperm whale (Physeteroidea indet.). Finally, the long-snouted archaic odontocete *Chilcacetus cavirhinus* is represented by two partial skeletons: 1) MUSM 1401, described by Lambert et al. (2015b); and 2) MUSM 2527, currently under study.

More than one thousand isolated elasmobranch teeth and spines, representative of at least nine families and sixteen different species, have been collected (Table 2 and Fig. 7). These remains belong to the following four orders: *i*) Carcharhiniformes (57.1% of the specimen), Lamniformes (35.2%), Myliobatiformes (7.5%), and Rhinopristiformes (0.2%) (Fig. 6C).

Carcharhiniformes are represented by seven species (*Carcharhinus brachyurus*, *Carcharhinus* cf. *leucas*, *Galeocerdo aduncus*, *Hemipristis serra*, *Negaprion brevirostris*, *Physogaleus contortus*, and *Sphyrna zygaena*), Lamniformes by seven (*Alopias superciliosus*, *Anotodus agassizii*, *Carcharias* sp., *Carcharocles chubutensis*, *Cosmopolitodus hastalis*, *Isurus oxyrinchus*, and *Megalolamna paradoxodon*), Myliobatiformes by one or more (Myliobatoidea indet.), and Rhinopristiformes by one (*Anoxypristis* sp.). Almost half of the elasmobranch remains consist of teeth of *C. brachyurus* (49.4%); teeth of *C. hastalis* (22.2%) and *I. oxyrhincus* (8.1%) follow in order of decreasing abundance.

Bony fish are represented by an indeterminate cranium, some very fragmentary tuna-like

skeletons, and the partial postcranial of a large istiophorid billfish tentatively referred to aff. *Makaira* sp. Similarly to the Pisco Formation (Collareta et al., 2015; Di Celma et al., 2017), cycloid scales consistent with those of the extant Pacific pilchard *Sardinops* are rather common in *Ct1a*.

Other marine vertebrates include a large dermochelyid marine turtle, represented by a single specimen consisting of some postcranial bones.

4.3. Distribution of the fossil vertebrates

Most of the fossils of vertebrates of Ullujaya come from a 1 km^2-surface area where the *Ct1a* is exposed (Fig. 2A); in turn, based on our field observations, both *Ct1b* and the Ct2 allomember of the Chilcatay Formation exposed in the study area seem devoid of vertebrate specimens preserved as bony elements. Vertebrate fossils have been found between 9.7 and 33.5 m abs, representing a significant portion of the 35 m-thick *Ct1a* (Fig. 6A). Seventy-four specimens (97 % of those with a stratigraphical collocation) are restricted in a 16.9 m-thick interval of sediments (13.9 to 30.8 m abs). The largest concentrations of fossil vertebrate remains are found between 14 and 15 m abs (22 specimens, 29%) and from 25 to 31 m abs (36 specimens, 7%). The large majority of the chondrichthyan specimens was collected from a single fossiliferous interval located about 23 m abs, whereas a few additional remains (mostly referable to *Cosmopolitodus* and *Carcharocles*) come from different horizons within *Ct1a*. Bony fish are homogeneously distributed between 14.2 m and 29.2 m abs, whereas the dermochelyid turtle specimen was found 14.8 m abs.

4.4. Physical taphonomy

Excluding twelve specimens that were not found *in situ* (due to recent erosion and subsequent dislocation), all the fossil vertebrate skeletons whose stratigraphic collocation is known display various degrees of disarticulation and are incomplete (Table 1 and Figs. 8, 9). The associated bones of the disarticulated skeletons exhibit a random disposition without any preferential orientation.

Among the sixteen cetacean crania found *in situ*, nine (56.2%) are disposed dorsal side-up and seven (43.8%) are disposed ventral side-up position (Fig. 8A). For most of the studied specimens, all skeletal elements are found within a single sediment layer, and evidence of sinking into the substratum are generally absent. Disarticulated vertebrae are typically observed with their epiphyseal surfaces parallel to the subjacent stratification – a disposition that would prove very stable for a vertebra resting for a prolonged time on a relatively compact soft substrate which does not allow sinking (Figs. 8B-E). The few exceptions include disarticulated vertebrae with transverse processes stuck into the underlying sediment (Figs. 9F, G) and a partly articulated vertebral column that moderately sank into the substratum (Figs. 9H, I).

Considering all the cetacean specimens that were found *in situ*, twenty-five of them (48.1%) consist of just one isolated anatomical element (e.g., cranium, vertebra, rib; Fig. 8A), thirteen (25.0%) of a few fully disarticulated bones (ca 25% of the skeleton being preserved; Figs. 8B-E), eleven (21.2%) of a few partially articulated bones (e.g., a few articulated vertebrae and ribs, with the remaining bones being disarticulated; Figs. 8F, G), two (3.8%) of fully disarticulated partial skeletons (ca 50% of the skeleton being preserved; Figs. 8H, I), and one (1.9%) of a fully articulated small portion of the skeleton (seven vertebrae; Figs. 8J, K). The articulation *vs* completeness bivariate bubble plot obtained with the above data (Fig. 10) highlights the high number of specimens whose completeness and articulation equal to zero. As a consequence, the T value is also very low (0.30), thus supporting biostratinomic conditions and processes favouring the disarticulation of the carcasses and the dispersal of the bony elements. The low value (0.08) of r^2 and the moderate (0.47) value of rs indicate that articulation and completeness are not firmly related to each other, as also evidenced by the observation of fully disarticulated skeleton with different degree of completeness.

Out of the thirteen cetacean skulls collected for systematic study, only one of them retains the mandible (but only the right ramus) articulated, only one has both periotics (ear bones) articulated,

one displays all the teeth in anatomical position, and six lack all teeth in their alveoli.

The smaller sample of non-mammalian vertebrates preserved as skeletal elements (one sea turtle and ten bony fish) confirms the taphonomic pattern observed for the cetaceans, all the detected skeletons being more or less incomplete and articulated. In particular, among bony fish, the most complete specimen (referred to aff. *Makaira* sp.) consists of an articulated, significant portion of the vertebral column with several skeletal elements scattered in a few square metres. The other fish specimens consist of six isolated portions of partly articulated vertebral columns (Figs. 9D, E), one fully articulated caudal fin (Fig. 9C), one isolated cranium, and two fragmentary portions of skulls.

Molluscs, barnacles, worm tubes, and other invertebrate remains, as well as shark teeth, are never found strictly associated to the bones. Bioerosion due to macro-invertebrates is never observed on the fossil bones, whereas shark bite marks are occasionally encountered (see paragraph 4.5). Bioturbations caused by the bone-eating worm *Osedax* (Kiel et al., 2010) and other evidences of whale fall communities (Smith et al., 2015) have not been observed. None of the detected specimens was found included and/or associated to carbonate concretions, unlike what has been observed in the overlying Pisco Formation (Gariboldi et al., 2015; Gioncada et al., 2016). Furthermore, macroscopic evidence of adhering phosphate crusts or envelopes has not been observed.

Macroscopically, most of the bones preserved within the sediment have a reddish colour and appear well mineralised. SEM-BSE observations on representative samples (Table 3) indicate that the bone tissue is rather dense (Figs. 11A, B), confirming a good degree of mineralisation, with well-preserved bone structures. Under the optical microscope, in both the compact and the cancellous bone, Haversian canals and medullary cavities may exhibit cementation (Table 3 and Figs. 11C-F). In one of the samples, Ca-phosphate partially fills osteon porosity, indicating incipient permineralisation. In several cases (Table 3), the Haversian canals of the compact bone and the larger medullary cavities of the cancellous bone are totally or partially filled by Ca-Mg carbonates.

Several generations of carbonate cement are observed, having different Ca/Mg ratios. Furthermore, in several samples, sediment grains fill some of the bone cavities, thus providing evidence that the bone went broken before diagenesis occurred. In some cases, Fe-oxides/hydroxides fill the Haversian canals in the reddish portions of the bone. Gypsum can also fill partly the bone cavities.

When the external part of the bone is preserved, it can be intact, partly dissolved, or affected by microborings. Two of the four examined specimens having bones not decorticated exhibit microborings of the B-type (*sensu* Gariboldi et al., 2015) (Table 3). In these cases, borings are a few μm wide and can be filled by gypsum, apatite, or Fe-oxyhydroxides. The boundary between the bone tissue and the sediment is cemented by Fe-oxyhydroxides causing the bone surface to appear reddish.

Field evidence of abrasion and fracturing of the exposed bones is often not easy to interpret due to the erosion in the present-day desert. In this respect, the analysis of thirteen partial skeletons collected for systematic study has proven more useful. Most of these fossils lack evidence of abrasion, having their cortical bone well preserved (e.g., the *Chilcacetus cavirhinus* MUSM 1401 and the *Huaridelphis raimondii* MUSM 1403). However, weak abrasion is observed in some crania of the MUSM collections (e.g., the *Kentriodon* MUSM 2431 and MUSM 631), but that could be due to recent erosion. Fracturing is clearly observed in one cranium (MUSM 631) referred to *Kentriodon*, having its posterior portion damaged (Figs. 12A, B). In all the other collected skulls, fractures (if present) are minor and do not generate significant distorsion of the bones (e.g., in the holotype skull MUSM 1396 of *Huaridelphis raimondii*, Figs. 12C, D). Delicate bone elements, such as the hamular processes and the laminae of the pterygoid, are preserved in several crania. With regard to the postcranial remains, most bones are broken and fragmentary (in part, because of recent erosion), although some vertebrae exhibit a good state of preservation of the narrow and elongated neural spine and transverse processes.

4.5. Shark bite marks

Although shark bite marks were not observed in the field on the exposed surfaces of bones, four of the specimens collected for systematic study are affected by these traces (Fig. 13).

Only one of the eleven collected crania exhibits bite marks. It consists of an isolated cranium referred to *Kentriodon* sp. (MUSM 1398) displaying two unserrated marks on the dorsal surface of the right premaxilla at mid-length of the rostrum (Fig. 13O). Considering that these traces are short (*ca* 5 mm long) and shallow, they are probably due to scavenging rather than to active predation. This hypothesis is consistent with the feeding behaviour of the extant white shark *Carcharodon carcharias*, which usually does not target the head region of dolphins in order to avoid biosonar detection (Long and Jones, 1996).

Two partial skeletons referred to *Chilcacetus cavirhinus* (MUSM 1401 and MUSM 2527) and one partial skeleton referred to *Huaridelphis raimondii* (MUSM 1403), exhibit bite marks on postcranial bones. Interestingly, to date, these three specimens are the only fossil vertebrates from Ullujaya for which significant postcranial material was collected, suggesting that bite marks could be relatively frequent on the postcranial remains of the Ullujaya odontocetes. The lack of field observations of bite marks could be favoured by the limited exposure of the bones and to the only partial preservation, due to recent erosion, of their cortical region.

The partial skeleton of *Chilcacetus cavirhinus* MUSM 2527 exhibits several bite marks on one of the three preserved ribs (Fig. 13A) and on the left humerus (Figs. 13B, C). Considering the unserrated nature and the size of these marks, all the bites observed on MUSM 2527 bones could have been inflicted by a young individual of *Cosmopolitodus hastalis*, a shark species known from *Ct1a* by abundant teeth. The (?)posterior rib is affected by several marks, the longest of which, about 20 mm long, are a type V bite mark (removing of a roughly prismatic or wedge-shaped chip of bone due to ubiquitous biting or as a result of a single cutting action directed deep into the bone; Collareta et al., 2017a) and two parallel type I marks (Cigala Fulgosi, 1990; Bianucci et al., 2010b).

The humerus is affected by two clusters of bite marks on the lateral and medial surfaces of the bone. Both clusters consist of several type I-II-III bite marks exhibiting a preferential orientation orthogonal to the main axis of the humerus, with several marks crossing each other. These marks are moderately deep, with lengths ranging from a few millimetres to 90 mm. They range in shape from rectilinear to weakly arched, their concavity being facing distally. The marks on the medial surface of the humerus are more numerous (ca 30) and generally more elongated than those on its lateral surface (ca 12). Although the skeleton of MUSM 1403 is rather incomplete, some speculations could be made about the trophic interaction between the shark(s) and the dolphin. The traces on the (?)posterior rib suggest an active attack from behind and below, a predation strategy documented for the extant white shark on pinnipeds and dolphins (Long and Jones, 1996; Klimley et al., 1996) and also suggested for other fossil cetaceans whose ribs display bite marks (Cigala Fulgosi, 1990; Bianucci et al. 2010b; Bianucci and Gingerich, 2011). This hypothesis is strengthened by the observation of a large number of marks, some of which are very deep (one even removing a chip of bone), indicating one or more powerful bites possibly causing the death of the dolphin. On the whole, the shape, size, and arrangement of the marks on the humerus suggest that a single shark grasped the flipper of the dolphin, trying to tear it off with repeated bites and by rotating the head (Fig. 13E). The greater number of traces on the medial surface of the humerus could be due to the greater number of functional teeth of the lower jaw of the shark as compared to the upper jaw (Fig. 13D), supposing that the dolphin was in a ventral up position. The pectoral fins are not included among the parts of the body of dolphins targeted by white sharks in active predation events (Long and Jones, 1996) suggesting that the bites on the humerus of MUSM 1403 were inflicted to the agonizing or even dead dolphin after a first attack to the abdomen (Figs. 13F, G). As young white sharks do not generally attack healthy cetaceans, and adult great whites only actively prey upon distinctly smaller food items (Long and Jones, 1996), it is possible that the odontocete individual MUSM 1403 was already weakened when the attack took place. However, as

in all documented cases of shark bite marks on fossil cetacean bones (Deméré and Cerutti, 1982; Cigala Fulgosi, 1990; Lambert and Gigase, 2007; Noriega et al., 2007; Ehret et al, 2009; Bianucci et al. 2010b; Bianucci and Gingerich, 2011; Collareta et al., 2017a), it is not easy to discriminate between marks being the result of active predation and marks resulting from scavenging on a carcass, either drifting at the water surface or lying along the seafloor.

The other partial skeleton of *Chilcacetus cavirhinus* (MUSM 1401) exhibits bite marks along the left mandible (Fig. 13H) and on the three preserved ribs (Figs. 13I-L). The marks on the left mandible are located on the lateral side of the symphyseal portion and consist of seven 4–7 mm-long unserrated incisions, six of which are type I bites inflicted almost perpendicular to the main axis of the bone, whereas another mark is a type V mark. Both the (?)second ribs are deeply incised with several bite marks. The (?)second left rib is almost complete and exhibits a high concentration of traces on its proximal posterior surface, where two deep, parallel, unserrated, *ca* 15-mm-long type I marks are observed alongside one irregular hole referable to the vertical impact of a shark tooth. The other marks are smaller and include a type III mark with parallel incisions produced by a serrated tooth. The longest traces on the fragmentary (?)second right rib are: 1) two (type II?) marks, 21 and 13 mm long respectively, on the proximal posterior surface of the bone, and 2) a type I or II mark, 16 mm long, on its anteroventral surface. The third incomplete rib exhibits some small type I marks on the dorsal surface and some weak incisions on the neck of the missing tubercle. The few long and deep unserrated marks detected on this bone, closely associated to several small and shallower traces (including one with serrated margins), suggest that the dolphin was first attacked or scavenged by one or more large lamniform sharks with non-denticulated teeth (e.g., *Cosmopolitodus*), then by smaller sharks (belonging to at least two different species) scavenging preferentially those parts of the carcass that were previously lacerated by stronger bites. Scavenging on cetaceans killed by other sharks is well documented in present-day mackerel sharks (Pratt et al., 1982; Casey and Pratt, 1985; Long and Jones, 1996).

Finally, the *Huaridelphis raimondii* partial skeleton MUSM 1403 exhibits some shallow incisions (most likely due to scavenging) near the end of a rib fragment (Fig. 13M) and two deep and short type I bite marks on the dorsal margin of another proximal rib fragment (Fig. 13N).

5. Discussion

5.1. Reconstruction of the depositional environment

Facies architecture, bedding patterns, and skeletal composition of the *Ct1b* clinoforms described here bear striking similarities with seaward-prograding mixed siliciclastic-carbonate wedges documented by Pomar and Tropeano (2001) and Massari and D'Alessandro (2012) and reflect the outwards dispersal of sediment in concert with the skeletal production rate and the available physical accommodation space (*sensu* Pomar and Kendall, 2008). According to these interpretations, *Ct1b* represents an entirely Submerged Infralittoral Prograding Wedge (ILPW; Hernández-Molina et al., 2000; Pomar et al., 2015), characterised by a storm-wave-graded profile, located at shoreface depth between the fair-weather and storm wave base, and distinctive clinoform foresets (Fig. 14). In this setting, high wave-current shear-stress in shoreface environment ensures that topsets of subaqueous clinoforms are regions of dominant sediment bypass through lateral advection, erosion, and redistribution. Accordingly, it is inferred that coarse-grained skeletal hash derived from a shallow-water carbonate factory inboard of the clinoform break-points was occasionally transported seawards and deposited on the sloping front of the ILPW separating the shoreface and the offshore (transition-slope setting of Pomar and Tropeano, 2001), leading to the formation of the clinoform foresets.

Downdip transport and dispersion of skeletal debris were especially active during storms by downwelling currents transforming into gravity flows at the clinoformed slope margin (Massari and Chiocci, 2006). At the same time, the winnowed-out fine-grained material actively bypassed the ILPW as part of the suspended load and was deposited farther downdip, into a deeper inner shelf

environment.

Basinward, these clinoformed skeletal-rich sediments interfinger with and downlap onto the vertebrate fossil-bearing siltstones and fine-grained sandstones of *Ct1a*. Given its downdip position with respect to the ILPW, *Ct1a* is considered to represent deposition by suspension fallout of shoreface-derived fine-grained material. The sharp-based, granule- to cobble-sized conglomerate beds interbedded into these fine-grained background sediments clearly reflect periodic high-energy events in otherwise quite marine offshore settings. Accordingly, they are interpreted as event beds resulting from tsunami backflows or storm-induced, offshore-directed density underflows transporting coarse-grained shoreface sediments beyond the toe of the transition slope. The exclusive association of discrete burrowed intervals with gravity-flow event beds intercalated in otherwise poorly bioturbated sediments and the restriction of burrow assemblages to *Thalassinoides* and *Gyrolithes* ichnogenera suggest a genetic relationship between bioturbation by decapod crustaceans and gravity flow deposition. As such, the *Thalassinoides*-*Gyrolithes*-burrowed intervals documented within *Ct1a* resemble the "doomed pioneers trace fossil assemblages" documented by Föllmi and Grimm (1990). In their doomed pioneer hypothesis, the authors argued that ichnofabrics beneath gravity-flow event beds deposited in generally inhospitable environments (e.g., benthic oxygen-deficiency) may be the product of adult allochtonous crustaceans that probably grew up in the well-oxygenated marginal areas and survived exhumation, transport by gravity-driven sediment flows, and re-deposition into deeper-water, oxygen-depleted depositional sites. Based on their interpretation, the displaced callianassid tracemakers are versatile enough to live and feed under the new oxygen-deficient bottom conditions for a short period of time before dying from suffocation and, therefore, may successfully penetrate the substrate to create conspicuous dwelling burrow networks. Accordingly, the systematic absence of additional ichnogenera and autochthonous body fossils of shelled benthic organisms throughout *Ct1a* supports the possibility that the *Thalassinoides*-*Gyrolithes*-burrowed intervals reflect short-term burrowing activity of doomed

pioneers in an otherwise oxygen-deficient sea-bottom environment normally inhibiting benthic life (Föllmi and Grimm, 1990).

Further supporting the hypothesis of poorly oxygenated bottom waters, we observed the presence of disseminated iron oxide framboids, which we interpret as relics of pyrite framboids, in the sediments of *Ct1a*. According to Agbi et al. (2015), the size distribution of framboidal pyrite could be used for distinguishing between oxic-dysoxic and euxinic conditions in the palaeo-bottom water, using the method applied by Wilkin et al. (1996) in modern sediments. Wilkin et al. (1996) noticed that pyrite framboids from euxinic environments are generally smaller and less variable in size than those from sediments underlying oxic or dysoxic bottom water, and related this feature with the different formation mechanisms of pyrite (Raiswell and Berner, 1985), which is syngenetic in euxinic settings and diagenetic in sediments underlying oxic water columns. In the *Ct1a* sediments exposed at Ullujaya, the size distribution of ex-pyrite framboids suggests an alternation of periods characterised by euxinic and oxic-dysoxic conditions (Figs. 5, 15). As recorded in the modern euxinic environments (Wilkin et al., 1996), framboids from samples UL-D1, UL-D2, UJA-49, and UL-D5 exhibit a mean diameter close to 5.0 ± 1.7 μm and large (i.e., > 10 μm) framboids are scarce, accounting for less than 4% of the measured aggregates. Indeed, framboids from sample UL-D3 exhibit a mean diameter of 8.3 μm (± 4.8) and more than 30% of them is large-sized, in agreement with the description of pyrite aggregates from modern oxic-dysoxic environments, with a mean of 7.7 ± 4.1 μm and 10-50 % of framboids > 10 μm (Wilkin et al. 1996). Therefore, the *Ct1a* palaeoenvironment of Ullujaya was interested by some euxinic events; on the other hand, the marine fossil assemblages found in the Ct1 allomember, including bivalves and barnacles in the shallow-water *Ct1b* and fish and cetaceans in the inner shelf *Ct1a*, suggest normal oxygenation in nearshore areas, where breaking waves efficiently mixed oxygen from the atmosphere into the water.

A key role in the development of oxygen-deficient conditions on the sea floor was probably

played by local factors, such as the semi-enclosed nature of the EPB during deposition of the Chilcatay strata (Fig. 1B) and the likely presence of a nearby upwelling zone where deep, nutrient-enriched water raised towards the surface, causing increased organic productivity and high oxygen demand on the shelf, as observed along the present-day Eastern Pacific margin (Pickering et al., 1989). As a matter of fact, however, diatom forms that are typical of upwelling settings (e.g., *Thalassionema*) do not occur in Ct1, but they are present in the overlying deposits of the Ct2 allomember.

The record of silicoflagellates from Ullujaya helps in further refining our reconstruction of the depositional environment. The silicoflagellate assemblage from *Ct1a* features the temperate genus *Distephanopsis*, the warm-water genera *Corbisema* and *Naviculopsis*, and the cold-water genus *Stephanocha*. This assemblage is best interpretable as witnessing warm-temperate thermal conditions.

Finally, an approximate estimation of the palaeobathymetry recorded by the toe of the slope at the transition between *Ct1a* and *Ct1b* can be obtained by summing up the depth of the break-points of the clinobedded units and the thickness of the clinobeds (15-20 m in *Ct1b*). The outer edge of the infralittoral wedge is naturally dependent on many different environmental factors, of which the wave climate, fetch, grain size, and general oceanographic conditions are among the most important (Mitchell et al., 2012). In the Mediterranean area, both Hernández-Molina et al. (2000) and Massari and Chiocci (2006) have found the outer edges of the breakpoints of the clinobedded units located at water depths of about 15–20 m. Due to the protected palaeogeography displayed by the EPB (Fig. 1B), the hydrodynamic conditions during deposition of the Chilcatay Formation would have been remarkably less energetic from those dictating the development of modern non-tropical skeletal carbonate sediments in oceanic settings exposed to vigorous storm-waves and probably resulted in the formation of prograding wedges at relatively shallower water depths. As a consequence, by assuming a water depth of the outer edge of the infralittoral wedge similar to that documented in the

Mediterranean area, an offshore depositional setting at least 30-40 m below the sea level can be interpreted for *Ct1a* at the toe of the slope.

The bioturbated nature of the lower boundary of the Ct2 allomember and its association with a basal oyster-bearing shelly horizon and a mixture of extrabasinal pebble- to boulder-size clasts, indicate that erosional scouring and shell concentration took place during a period of sea-level fall followed by transgression (e.g., Kidwell, 1991; Abbott, 1998; Carnevale et al., 2011).

5.2. Genesis of the marine vertebrate fossil assemblage

Our taphonomic observations and the reconstruction of the *Ct1a* depositional environment suggest prolonged flotation and repeated movements through the water mass of the marine vertebrate carcasses before their final deposition on the seafloor (Schäfer, 1972). During this long-time floating phase, the carcasses were subject to biogenic and physical processes of partial destruction, as supported by the shark bite marks (at least part of them indicating scavenging action) and by the overall low degrees of completeness and articulation of the specimens. The high number of isolated crania of cetaceans may record the separation of the relatively heavy head from the rest of the body during the early phases of the flotation of the carcasses, as observed by Schäfer (1972) for extant dolphins and already hypothesised for fossil cetaceans from the upper Miocene of the EPB by Bianucci et al. (2010a). Further disarticulation could have occurred during the period when the carcasses laid exposed on the seafloor, due to the fluidization of the remaining soft tissues and consequent gravitational collapse (Reisdorf et al., 2014). In some cases, the presence of sediment infilling some bone cavities proves that the micro-breakages of the bones occurred before diagenesis and that bones were exposed on the seafloor after the carcass deposition, as a consequence of the early body dismemberment.

Bottom currents can be discarded as a cause of disarticulation due to the lack of preferential orientation of the disarticulated remains and the lack of sedimentary structures, considering also that

the aforementioned evidence of euxinic conditions supports water stagnation close to the seafloor. Together with the scarcity of breakage and abrasion marks on the bones, the preservation of delicate bone structures further supports the absence of transport due to bottom currents. Scavenging action as a cause of disarticulation can be discarded due to the lack of fossil traces on the bones (with the notable exception of those left by sharks) and of closely associated macroinvertebrate remains (whose absence is probably due to the euxinic conditions of the bottom waters, see above).

Bones often exhibit a reddish colour on the surface, visible at both macro- and micro-scale (Figs. 11C-F and 13). This feature is probably due to the oxidation of Fe, available for the formation of abundant pyrite framboids in anoxic bottom water and within the sediments.

Bone cavities, such as Haversian canals and medullary cavities, show in some cases a Ca-phosphate filling that occurred during early diagenesis and a later cementation of carbonates (spatic calcite and subordinate Mg-Ca carbonates) or gypsum. Differing from what has been recorded at various sites of the Pisco Formation, micritic clotted dolomite filling the bone cavities and dolomite envelopes have not been observed with fossil vertebrates at Ullujaya. In the deposits of the Pisco Formation, dolomite concretions grew around vertebrate carcasses during the very early phases of diagenesis, as a consequence of anaerobic degradation processes of organic matter leading to cementation of the surrounding matrix (Gariboldi et al., 2015; Gioncada et al., 2016, 2018). Therefore, the formation of dolomite nodules requires an early covering of the vertebrate carcass by sediment (e.g., via sinking into a soupy substrate or rapid burial by high rates of sediment deposition) (Gariboldi et al., 2015; Gioncada et al., 2016). Moreover, microbially mediated degradation processes inducing dolomite precipitation are more likely to be efficient if the amount of decaying organic matter is large and permeability of the embedding sediment is low, both conditions favouring a locally anoxic environment (Gioncada et al., 2018). At Ullujaya, taphonomic and sedimentological evidence accounts against rapid sinking and/or burial of the vertebrate carcasses, supporting instead the hypothesis that their deposition occurred after substantial

defleshing and the consequent exposure of the bones on the seafloor. Such a prolonged biostratinomic journey likely contributed to prevent the formation of dolomite envelopes around the Ullujaya marine vertebrate remains.

The fine-quality preservation of the bones, the absence of adhering phosphate crusts or nodules, and the above reported sedimentary evidence also exclude the interpretation of the *Ct1a* vertebrate assemblage as a condensed deposit due to hiatal and/or lag concentration consequent to low sedimentation rates or erosion (see Pyenson et al., 2009; Boessenecker et al., 2014).

5.3. Stratigraphic significance and comparison with other coeval vertebrate assemblages

5.3.1. Cetaceans

At the species level, the Ullujaya assemblage shares the squalodelphinid *Notocetus vanbenedeni* with the Aquitanian–lower Burdigalian Leonian assemblage, Argentina (Cozzuol, 1996). Similarly, both faunas include a species of *Kentriodon*, and a physeteroid from Ullujaya displays similarities with the Leonian *Diaphorocetus poucheti*. A squalodelphinid and a physeteroid are also recorded in the upper Aquitanian-lower Burdigalian Belluno assemblage, Italy (Bianucci and Landini, 2002), whereas at least one squalodelphinid and *Kentriodon* are known from the lower Miocene formations of the eastern U.S.A (Kellogg, 1932; Whitmore and Kaltenbach, 2008; Kidwell et al., 2015; Boessenecker, 2018). Finally, the long-snouted homodont odontocete *Chilcacetus cavirhinus* may belong to the same clade as the Leonian *Argyrocetus patagonicus* and several species from the Aquitanian Pyramid Hill assemblage, California, U.S.A. (Lambert et al., 2015b).

Interestingly, the Ullujaya assemblage features no mysticetes, a condition shared by all other coeval sites, a main exception being the Leonian assemblage, which includes one 'cetothere' and one balaenid (Buono et al., 2017). The Aquitanian gap in the mysticete fossil record could partly reflect a limited number of cetacean-bearing localities (Marx and Fordyce, 2015). The low diversity of early Miocene filter-feeding mysticetes may also be correlated to a drop in diatom diversity that

would have particularly impacted cetaceans preying upon small-sized prey (Marx and Uhen, 2010). The fact that the Argentinian localities are the southernmost among these lower Miocene assemblages may suggest that the circum-Antarctic areas were refuge regions for mysticetes at that time.

5.3.2 Elasmobranchs

Many elasmobranch taxa found at Ullujaya are stratigraphically uninformative, being common components of Neogene chondrichthyan assemblages from shallow-marine settings worldwide. Most of them are also known from the late Miocene deposits of the EPB (Di Celma et al., 2017; Landini et al., 2017a). However, two otodontid taxa (*Megalolamna paradoxodon* and *Carcharocles chubutensis*) are of particular stratigraphic interest. *M. paradoxodon* is known from a few localities worldwide, being seemingly limited to the Aquitanian–Burdigalian interval (Shimada et al., 2017). In turn, *Carcharocles* is one of the most ubiquitous and widespread Neogene elasmobranch genera. Pimiento et al. (2016) suggested that *Carcharocles* represents a lineage of chronospecies whose latest representatives are *C. chubutensis* (making its last appearance in Oligocene or earliest Miocene times) and the late early Miocene–Pliocene *C. megalodon* (whose presence in Burdigalian deposits has been demonstrated by Carrillo-Briceño et al., 2015). The present report of remains of *C. chubutensis* (including fragmentary adult teeth, always displaying lateral cusplets) from Ullujaya could suggest that *C. chubutensis* and *C. megalodon* coexisted during the late early Miocene (see also Aguilera and Aguilera, 2004). On the other hand, *C. chubutensis* and *C. megalodon* are not found together in the EPB, as *C. megalodon* is absent from the Chilcatay Formation, being in turn the sole otodontid featured in the geologically younger Pisco Formation (Landini et al., 2018).

5.3.3 Bony fish

Both the family Istiophoridae and the scombrid genus *Thunnus* are known from the Eocene onwards (Fierstine, 2006; Santini et al., 2013). Fossil pilchards are very rare in the Pacific realm, and the origin itself of the genus *Sardinops* is only tentatively referred to the early Miocene (Parrish

et al., 1989). Tuna-like fish, marlins, and *Sardinops* are also known from the upper Miocene strata of the EPB (Collareta et al., 2015, 2017b; Lambert et al., 2015a; Bianucci et al., 2016a; Di Celma et al., 2017).

5.3.4 Turtles

The fossil history of dermochelyids spans from the Palaeocene onwards (Delfino et al., 2013). A dermochelyid turtle (*Natemys peruvianus*) has been described based on a partial shell from the "Late Oligocene Pisco Formation […] approximately 1.5 km southwest of Hacienda Ullujaya" (Wood et al., 1996). Based on our observations, only the Chilcatay Formation is exposed at that locality; that would also account better for the proposed Oligocene age of *Natemys peruvianus*.

5.4. Vertebrate palaeoecology

5.4.1. Cetaceans

Palaeoecological analyses of fossil cetacean assemblages must account for some major caveats. First, floating cetacean carcasses can suffer substantial transport by marine or fluvial currents before depositing at the seafloor (Schäfer, 1972). Second, the reconstruction of the feeding and habitat preferences of fossil cetaceans is not obvious when the fossil taxa do not have close and phenetically similar extant relatives (e.g., *Chilcacetus* and cf. *Diaphorocetus*). Third, the absence of some significant clades of large-sized cetaceans (e.g., mysticetes) could reflect long-term biogeographical patterns rather than eco-environmental constraints. Finally, some of the Ullujaya fossil cetaceans could have entered accidentally, as living organisms, into the sheltered *Ct1a* area from adjacent fluvial or pelagic environments. Given these limitations, the reconstructed scenario of Figure 14 should be regarded as partly speculative. However, we are confident that at least the small dolphin *Kentriodon*, the most common cetacean in *Ct1a*, likely lived in this area.

Most of the Ullujaya cetaceans (*Chilcacetus*, *Huaridelphis*, *Kentriodon*, and *Notocetus*) exhibit narrow rostra and small teeth; moreover, they are homodont and polydont, thus suggesting a

raptorial feeding specialization for capturing small prey (e.g., small-sized fish and shrimps). Taphonomic selection, preventing the preservation of the delicate skeletons of small-sized vertebrates and decapods, could account for the apparent lack of fossils of these hypothetical prey items at Ullujaya. Given its very elongated and narrow rostrum and symphyseal portion of the mandibles, *Chilcacetus cavirhinus* could have been a coastal bottom-feeder (as the extant river dolphins) or an epipelagic piscivore (as hypothesised for the similarly long-snouted late Miocene beaked whale *Messapicetus gregarius*: Lambert et al., 2015a; Ramassamy et al., 2018). In both hypotheses, the long-snouted condition could have been driven by dietary preferences (e.g., a predilection for small fish) rather than by environmental conditions (McCurry et al., 2017).

The physeteroid cranium referred to cf. *Diaphorocetus* displays deep dental alveoli indicating a complete upper dentition and evoking a raptorial feeding behaviour that contrasts with the suction feeding technique of extant sperm whales. Compared to the size of the skull, the diameter of the alveoli is small, suggesting that this odontocete fed on smaller prey than other macroraptorial physeteroids (e.g., the large-toothed *Acrophyseter* and *Livyatan*: Lambert et al., 2017).

The Ullujaya vertebrate assemblage does not feature two recently described Chilcatay odontocetes, namely, the possibly suction feeding *Inticetus* (Lambert et al., 2018) and the macroraptorial squalodelphinid *Macrosqualodelphis* (Bianucci et al., 2018). This observation indicates that the morphological and ecological disparity of the Chilcatay cetaceans is greater than that recorded at Ullujaya.

5.4.2. Elasmobranchs

The Ullujaya elasmobranch assemblage is dominated by remains of *Carcharhinus brachyurus*, which currently inhabits warm-temperate waters 0–100 m deep (Compagno, 1984). *Carcharhinus brachyurus* occasionally occurs in brackish and estuarine waters and elects semi-enclosed embayments as nursery grounds (Duffy and Gordon, 2003). A shallow-water environment is also supported by the presence of *Negaprion brevirostris* and *Carcharhinus* cf. *leucas*, two strongly

littoral, tropical-subtropical carcharhinids that thrive in mangrove swamps and river mouths (Compagno, 1984; Compagno and Niem, 1998). Similarly, *Anoxypristis* is a nectobenthic organism that is found in coastal and estuarine warm-water environments (D'Anastasi et al., 2013). In turn, strong connections with the pelagic realm are supported by the presence of *Alopias superciliosus.* All the recognised extant taxa are nevertheless consistent with a coastal environment. A predilection for coastal warm-temperate habitats is also regarded as characteristic of the extinct species *Carcharocles chubutensis*, *Megalolamna paradoxodon*, and *Hemipristis serra*; moreover, the extant *Hemipristis elongata* is a tropical coastal shark that inhabits waters up to 30 m depth (Compagno, 1984). The ontogenetic structure of the observed assemblage also suggests a shallow coastal environment, as *Carcharhinus brachyurus* and *Cosmopolitodus hastalis* are mostly represented by juvenile teeth, thus evoking the presence of overlapping coastal nurseries (e.g., Landini et al., 2017b, 2018). *Alopias superciliosus*, *Carcharhinus brachyurus*, *Isurus oxyrinchus, Negaprion brevirostris*, and *Sphyrna zygaena* mostly rely on small- to medium-sized fish and subordinate cephalopods and crustaceans, and similar considerations apply to the extant species of *Carcharias* and *Hemipristis* (Compagno, 1984, 2001; Cortés and Gruber, 1990; Devadoss and Chandrasekar, 1991; Smale, 1991; Duffy and Gordon, 2003; Manojkumar and Pavithran, 2004; Cailliet et al., 2009). In turn, the more diverse trophic habits of *Carcharhinus leucas* and extant *Galeocerdo* include occasional predation upon marine tetrapods (including diminutive cetaceans) (Simpfendorfer and Burgess, 2009). *Anotodus agassizii* and *Cosmopolitodus hastalis* have been interpreted as eurytrophic littoral predators whose adult stages foraged mostly on fish while secondarily preying on diminutive marine tetrapods (e.g., Landini et al., 2017a). Among Otodontidae, *Megalolamna* is regarded as a piscivore which relied on medium-sized fish (Shimada et al., 2017), whereas the diet of *Carcharocles* was likely similar to that of extant *Carcharodon* – i.e., characterised by a high contribution of marine mammals (Collareta et al., 2017a).

As reported above, shark bite marks have been detected on some odontocete bones from

Ullujaya. These bones are referable to cetaceans roughly ranging in size between 1.5 m (*Kentriodon*) and 3.2 m (*Chilcacetus*). This size range overlaps with that of the known cetacean prey of large individuals of extant white sharks (e.g., Long and Jones, 1996). The bite marks are mostly referable to sharks with unserrated teeth. Smooth-edged teeth of *C. hastalis* are among the most common fossils at Ullujaya; this species presumably attained maximum size values comparable to those of the largest extant lamnids (Purdy et al., 2001). It is thus likely that *C. hastalis* was the most prominent predator of cetaceans in the Ullujaya palaeoecosystem. However, most of the *C. hastalis* teeth from Ullujaya belong to immature individuals, and juveniles of this species may have focused their diet on fish (Collareta et al., 2017b). Therefore, considering that large teeth referable to full-grown lamniforms (including also *C. hastalis*) are occasionally found all along the studied section, and taking also into account that extant mackerel sharks do not actively prey upon animals from their own size class, the most efficient predators of cetaceans at Ullujaya should have included large, transient individuals of *C. hastalis*. Bites due to scavenging on floating carcasses should also be taken into account, as it is known that large-sized white sharks feature a significant component of cetacean carrion in their diet (Long & Jones, 1996; Fallows et al., 2013).

Among rays, forms such as *Myliobatis* and *Anoxypristis* forage mainly on bentho-demersal prey, including hard-shelled invertebrates, fish, and squids (e.g., Jardas et al., 2004; Peverell, 2009: Molina and Cazorla, 2015; Rezende et al., 2015).

The Ullujaya elasmobranch assemblage is thus dominated by mesopredators, i.e., by juveniles and adults of species whose mature stages mainly relied on fish and macro-invertebrates and by juveniles of top-predator species (e.g., juveniles of *C. hastalis*) whose adult stages featured a significant component of marine tetrapods in their diet.

5.4.3 Bony fish

The co-occurrence of two families of primarily oceanic bony fish (Istiophoridae and Scombridae) supports connection with the open-ocean environment. Extant marlins are generally

close to the apex of pelagic food pyramids (Kitchell et al., 2006), their diet including large-sized bony fish such as mackerels, whereas tuna-like scombrids are opportunistic predators that feed at a slightly lower trophic level (Bertrand et al., 2002). Pilchards are small-sized epipelagic schooling fishes that inhabit highly productive coastal-pelagic environments and may enter semi-enclosed embayments; huge populations of *Sardinops* inhabit the present-day waters off Peru and represent a key prey item for other vertebrates (Chavez et al., 2003). Strong fossil evidence indicates that, during the late Miocene, *Sardinops* occupied a prominent position in the trophic chains of the EPB (Collareta et al., 2015, 2017b; Lambert et al., 2015). Pilchards likely also represented a fundamental trophic link at Ullujaya in Burdigalian times, although they were perhaps more common seawards of the Gran Tablazo Archipelago.

5.4.4 Turtles

The sole extant dermochelyid, *Dermochelys coriacea*, is a strongly pelagic organism that feeds on gelatinous invertebrates (Eckert et al., 2012). A dermochelyid in the semi-enclosed embayment of Ullujaya could suggest the presence of a nesting site in proximity of this area. Indeed, extant dermochelyids elect coarse-grained beaches (sometimes within protected embayments) with little abrasive clasts (e.g., coral fragments), and a steep approach to the sea as nesting sites (COSEWIC, 2012).

6. Conclusions

We investigated an early Miocene (Burdigalian) vertebrate assemblage dominated by diverse toothed cetaceans and elasmobranchs from the *Ct1a* facies association of the Chilcatay Formation of southern Peru.

Based on sedimentological, ichnological, and palaeontological considerations, *Ct1a* represents a sandy-silty sediment wedge deposited in a warm-temperate, 30-40 m in water depth, semi-enclosed embayment, connected with riverine and open-ocean environments and with recurrent euxinic

conditions at the seafloor.

Vertebrate skeletons are typically disarticulated and incomplete, and some of these are affected by shark bite marks. Bioerosion due to macro-invertebrates is never observed and none of the specimens was found included and/or associated to carbonate concretions.

A long-time floating phase allowed biogenic and physical partial destruction of the carcasses before deposition on a soft compact substrate. Oxygen-deficient bottom conditions inhibited the scavenging action of benthic organisms.

Acknowledgments and funding

We thank T. J. DeVries, F. G. Marx, K. Post, R. Salas-Gismondi, M. Martínez-Cáceres, V. Pacheco, and J. Tejada for their help during multiple field prospections and several fruitful discussions. Special gratitude to W. Aguirre and E. Díaz, for field assistance and fossil preparation. Thanks also to V. Barberini for the help with the radiometric analyses. Comments and suggestions by T. J. Algeo, R. W. Boessenecker, H. Falcon-Lang, and an anonymous reviewer greatly improved the quality of this work.

This study was supported by a grant from the Italian Ministero dell'Istruzione, dell'Università e della Ricerca [PRIN Project, 2012YJSBMK] to G. Bianucci, E. Malinverno, and C. Di Celma, two grants from the National Geographic Society Committee for Research Exploration to G. Bianucci [9410–13] and to O. Lambert [GEFNE177-16], and a grant by the University of Pisa to G. Bianucci [PRA_2017_0032]. Field work by O. Lambert, C. de Muizon, and G. Bianucci in 2010 and 2011 was supported by the Action Thématique Muséum (ATM) ‘Etat et structure phylogénétique de la biodiversité actuelle et fossile’ and by the Centre National de la Recherche Scientifique (CNRS), with logistical support of the Institut Français d’Etudes Andines (IFEA) and of the Institut de Recherche pour le Développement (IRD).

References

Abbott, S.T. (1998). Transgressive systems tract and onlap shellbeds from mid-Pleistocene sequences, Wanganui Basin, New Zealand. *Journal of Sedimentary Research*, 68, 253-268.

Agbi, I., Ozibo, B., Newton, R. (2015). Pyrite framboid size distribution of the Grey Shales (Yorkshire UK) as an indication of redox conditions. *IOSR Journal of Applied Geology and Geophysics*, 3, 36-42.

Aguilera, O.A., Aguilera, D.R. (2004). Giant-toothed white sharks and wide-toothed mako (Lamnidae) from the Venezuela Neogene: their role in the Caribbean, shallow-water fish assemblage: *Caribbean Journal of Science*, 40, 368-382.

Beardmore, S. R., Furrer, H. (2016a). Taphonomic analysis of *Saurichthys* from two stratigraphic horizons in the Middle Triassic of Monte San Giorgio, Switzerland. *Swiss Journal of Geosciences*, 109, 1-16.

Beardmore, S. R., Furrer, H. (2016b). Evidence of a preservational gradient in the skeletal taphonomy of Ichthyopterygia (Reptilia) from Europe. *Palaeogeography, Palaeoclimatology, Palaeoecology*, 443, 131-144.

Beardmore, S. R., Orr, P. J., Manzocchi, T., Furrer, H., Johnson, C. (2012). Death, decay and disarticulation: modelling the skeletal taphonomy of marine reptiles demonstrated using *Serpianosaurus* (Reptilia; Sauropterygia). *Palaeogeography, Palaeoclimatology, Palaeoecology*, 337, 1-13.

Bertrand, A., Bard, F. X., Josse, E. (2002). Tuna food habits related to the micronekton distribution in French Polynesia. *Marine Biology*, 140, 1023-1037.

Bianucci, G., Bosio, G., Malinverno, E., Muizon, C. de, Villa, I. M., Urbina, M., Lambert, O. (2018). A new large squalodelphinid (Cetacea, Odontoceti) from Peru sheds light on the Early Miocene platanistoid disparity and ecology. *Royal Society Open Science*, 5, article #172302.

Bianucci, G., Di Celma, C., Collareta, A., Landini, W., Post, K., Tinelli, C., Muizon, C. de, Bosio,

G., Gariboldi, K., Gioncada, A., Malinverno, E., Cantalamessa, G., Altamirano-Sierra, A., Salas-Gismondi, R., Urbina, M., Lambert, O. (2016a). Fossil marine vertebrates of Cerro Los Quesos: Distribution of cetaceans, seals, crocodiles, seabirds, sharks, and bony fish in a late Miocene locality of the Pisco Basin, Peru. *Journal of Maps*, 12, 1037-1046.

Bianucci, G., Di Celma, C., Landini, W., Post, K., Tinelli, C., Muizon, C. de, Gariboldi, K., Malinverno, E., Cantalamessa, G., Gioncada, A., Collareta, A., Salas-Gismondi, R., Varas-Malca, R.M., Urbina, M., Lambert, O. (2016b). Distribution of fossil marine vertebrates in Cerro Colorado, the type locality of the giant raptorial sperm whale *Livyatan melvillei* (Miocene, Pisco Formation, Peru). *Journal of Maps*, 12, 543-557.

Bianucci, G., Gingerich, P.D. (2011). *Aegyptocetus tarfa*, n. gen. et sp. (Mammalia, Cetacea), from the middle Eocene of Egypt: clinorhynchy, olfaction, and hearing in a protocetid whale. *Journal of Vertebrate Paleontology*, 31, 1173-1188.

Bianucci, G., Lambert, O., Post, K. (2010a). High concentration of long-snouted beaked whales (genus *Messapicetus*) from the Miocene of Peru. *Palaeontology*, 53, 1077-1098.

Bianucci, G., Landini, W. (2002). Change in diversity, ecological significance and biogeographical relationships of the Mediterranean Miocene toothed whale fauna. *Geobios*, 35, 19-28.

Bianucci, G., Urbina, M., Lambert, O. (2015). A new record of *Notocetus vanbenedeni* (Squalodelphinidae, Odontoceti, Cetacea) from the early Miocene of Peru. *Comptes Rendus Palevol*, 14, 5-13.

Bianucci, G., Sorce, B., Storai, T., Landini, W. (2010b). Killing in the Pliocene: shark attack on a dolphin from Italy. *Palaeontology*, 53, 457-470.

Boessenecker, R. W. (2018). Problematic archaic whale *Phococetus* (Cetacea: Odontoceti) from the Lee Creek Mine, North Carolina, USA, with comments on geochronology of the Pungo River Formation. *PalZ*. doi: 10.1007/s12542-018-0419-3

Boessenecker, R.W., Perry, F. A., Schmitt, J. G. (2014). Comparative taphonomy, taphofacies, and

bonebeds of the Mio-Pliocene Purisima Formation, Central California: strong physical control on marine vertebrate preservation in shallow marine settings. *PLOS ONE*, 9, article #e91419.

Buono, M.R., Fernández, M.S., Cozzuol, M.A., Cuitiño, J.I., Fitzgerald, E.M. (2017). The early Miocene balaenid *Morenocetus parvus* from Patagonia (Argentina) and the evolution of right whales. *PeerJ*, 5, article #e4148.

Cailliet, G.M., Cavanagh, R.D., Kulka, D.W., Stevens, J.D., Soldo, A., Clo, S., Macias, D., Baum, J., Kohin, S., Duarte, A., Holtzhausen, J.A., Acuña, E., Amorim, A., Domingo, A. (2009). *Isurus oxyrinchus*. In: The IUCN Red List of Threatened Species 2009: e.T39341A10207466. http://www.iucnredlist.org, accessed on April 28, 2018.

Carnevale, G., Landini, W., Ragaini, L., Di Celma, C., Cantalamessa, G. (2011). Taphonomic and paleoecological analyses (mollusks and fishes) of the Sua member condensed shellbed, Upper Onzole Formation (early Pliocene, Ecuador). *Palaios*, 26: 160-172.

Carrillo-Briceño, J.D., Maxwell, E., Aguilera, O.A., Sánchez, R., Sánchez-Villagra, M.R. (2015). Sawfishes and other elasmobranch assemblages from the Mio-Pliocene of the South Caribbean (Urumaco Sequence, Northwestern Venezuela). *PLOS ONE*, 10, article #e0139230.

Casey, J.G., Pratt Jr, H.L. (1985). Distribution of the white shark, *Carcharodon carcharias*, in the western North Atlantic. *Memoirs of the Southern California Academy of Sciences*, 9, 2-14.

Chavez, F.P., Ryan, J., Lluch-Cota, S.E., Ñiquen, M. (2003). From anchovies to sardines and back: multidecadal change in the Pacific Ocean. *Science*, 299, 217-221.

Cigala Fulgosi, F. (1990). Predation (or possible scavenging) by a great white shark on an extinct species of bottlenosed dolphin in the Italian Pliocene. *Tertiary Research*, 12, 17-36.

Clarke, J.A., Ksepka, D.T., Salas-Gismondi, R., Altamirano, A.J., Shawkey, M.D., D'Alba, L., Vinther, J., DeVries, TJ., Baby, P. (2010). Fossil evidence for evolution of the shape and color of penguin feathers. *Science*, 330, 954-957.

Clift, P.D., Pecher, I., Kukowski, N., Hampel, A. (2003). Tectonic erosion of the Peruvian Forearc,

Lima Basin, by steady-state subduction and Nazca Ridge collision. *Tectonics*, 22, article #1023.

Collareta, A., Lambert, O., Landini, W., Di Celma, C., Malinverno, E., Varas-Malca, R., Urbina, M., Bianucci, G. (2017a). Did the giant extinct shark *Carcharocles megalodon* target small prey? Bite marks on marine mammal remains from the late Miocene of Peru. *Palaeogeography, Palaeoclimatology, Palaeoecology*, 469, 84-91.

Collareta, A., Landini, W., Chacaltana, C., Valdivia, W., Altamirano-Sierra, A., Urbina, M., Bianucci, G. (2017b). A well preserved skeleton of the fossil shark *Cosmopolitodus hastalis* from the late Miocene of Peru, featuring fish remains as fossilized stomach contents. *Rivista Italiana di Paleontologia e Stratigrafia*, 123, 11-22.

Collareta, A., Landini, W., Lambert, O., Post, K., Tinelli, C., Di Celma, C., Panetta, D., Tripodi, M., Salvadori, P.A., Caramella, D., Marchi, D., Urbina, M., Bianucci, G. (2015). Piscivory in a Miocene Cetotheriidae: first record of fossilized stomach content for an extinct baleen-bearing whale. *The Science of Nature*, 102, article #70.

Compagno, L.J.V. (1984). FAO Species Catalogue. Vol 4: Sharks of the world, Part 1 - Hexanchiformes to Lamniformes. *FAO Fisheries Synopsis*, 125, 4, 1-250.

Compagno, L.J.V. (2001). Sharks of the world. An annotated and illustrated catalogue of shark species known to date. Volume 2. Bullhead, Mackerel and Carpet Sharks (Heterodontiformes, Lamniformes and Orectolobiformes). FAO, Rome.

Compagno, L.J.V., Niem, V.H. (1998). Carcharhinidae. In: K.E. Carpenter and V.H. Niem (eds.), FAO Identification Guide for Fishery Purposes. The Living Marine Resources of the Western Central Pacific. Food and Agriculture Organization, Rome, 1312-1324.

Cortés, E., Gruber, S.H. (1990). Diet, feeding habits, and estimates of daily ration of young lemon sharks, *Negaprion brevirostris* (Poey). *Copeia*, 1990, 204-218.

COSEWIC [Committee on the Status of Endangered Wildlife in Canada] (2012). COSEWIC assessment and status report on the leatherback sea turtle *Dermochelys coriacea* Atlantic

Population Pacific Population in Canada – 2012.https://www.registrelep-sararegistry.gc.ca/default.asp?lang=En&n=9F76DBB0-1, accessed on May 1, 2018.

Cozzuol, M. (1996). The record of aquatic mammals in southern South America. *Münchner Geowissenchaftliche, Abhandlungen, Rheihe A*, 30, 321-342.

D'Anastasi, B., Simpfendorfer, C., van Herwerden, L. (2013). *Anoxypristis cuspidata*. In: The IUCN Red List of Threatened Species 2013: e.T39389A18620409. http://www.iucnredlist.org, accessed on April 28, 2018.

Danise, S., Dominici, S. (2014). A record of fossil shallow-water whale falls from Italy. *Lethaia*, 47, 229-243.

Delfino, M., Scheyer, T. M., Chesi, F., Fletcher, T., Gemel, R., MacDonald, S., Rabi, M., Salisbury, S. W. (2013). Gross morphology and microstructure of type locality ossicles of *Psephophorus polygonus* Meyer, 1847 (Testudines, Dermochelyidae). *Geological Magazine*, 150, 767-782.

Deméré, T.A., Cerutti, R.A. (1982). A Pliocene shark attack on a cethotheriid whale. *Journal of Paleontology*, 56, 1480-1482.

Devadoss, P., Chandrasekhar, S. (1991). A note on the rare snaggle tooth shark, *Hemipristis elongatus*. *Marine Fisheries Information Service, Technical and Extension Series*, 114, 36.

DeVries, T.J. (1998). Oligocene deposition and Cenozoic sequence boundaries in the Pisco Basin. *Journal of South American Earth Sciences*, 11, 217-231.

DeVries, T.J. (2017). Eocene stratigraphy and depositional history near Puerto Caballas (East Pisco Basin, Peru). *Boletín de la Sociedad Geológica del Perú*, 112, 39-52.

DeVries, T.J., Jud, N.A. (2018). Lithofacies patterns and paleogeography of the Miocene Chilcatay and lower Pisco depositional sequences (East Pisco Basin, Peru). *Boletín de la Sociedad Geológica del Perú*, Volumen Jubilar 8, 124-167.

DeVries, T.J., Urbina, M., Jud, N.A. (2017). The Eocene-Oligocene Otuma depositional sequence (East Pisco Basin, Peru): paleogeographic and paleoceanographic implications of new data.

Boletín de la Sociedad Geológica del Perú, 112, 14-38.

Di Celma, C., Malinverno, E., Bosio, G., Collareta, A., Gariboldi, K., Gioncada, A., Molli, G., Basso, D., Varas-Malca, R.M., Pierantoni, P.P., Villa I.M., Lambert, O., Landini, W., Sarti, G., Cantalamessa, G., Urbina, M., Bianucci, G. (2017). Sequence stratigraphy and paleontology of the upper Miocene Pisco Formation along the western side of the lower Ica valley (Ica Desert, Peru). *Rivista Italiana di Paleontologia e Stratigrafia*, 123, 255-274.

Di Celma, C., Malinverno, E., Cantalamessa, G., Gioncada, A., Bosio, G., Villa, I.M., Gariboldi, K., Rustichelli, A., Pierantoni, P.P., Landini, W., Tinelli, C., Collareta, A., Bianucci, G. (2016a). Stratigraphic framework of the late Miocene Pisco Formation at Cerro Los Quesos (Ica Desert, Peru). *Journal of Maps*, 12, 1020-1028.

Di Celma, C., Malinverno, E., Collareta, A., Bosio, G., Gariboldi, K., Lambert, O., Landini, W., Pierantoni, P.P., Gioncada, A., Villa, I.M., Coletti, G., Muizon, C. de, Urbina, M., Bianucci, G. (2018). Facies analysis, stratigraphy and marine vertebrate assemblage of the lower Miocene Chilcatay Formation at Ullujaya (Pisco basin, Peru). *Journal of Maps*, 14, 257-268.

Di Celma, C., Malinverno, E., Gariboldi, K., Gioncada, A., Rustichelli, A., Pierantoni, P.P., Landini,W., Bosio, G., Tinelli, C., Bianucci, G. (2016b). Stratigraphic framework of the late Miocene to Pliocene Pisco Formation at Cerro Colorado (Ica Desert, Peru). *Journal of Maps*, 12, 515-557.

Duffy, C., Gordon, I. (2003). *Carcharhinus brachyurus*. In: The IUCN Red List of Threatened Species 2003: e.T41741A10551730. http://www.iucnredlist.org, accessed on April 28, 2018.

Dunbar, R.B., Marty, R.C., Baker, P.A. (1990). Cenozoic marine sedimentation in the Sechura and Pisco basins, Peru. *Palaeogeography, Palaeoclimatology, Palaeoecology*, 77, 235-261.

Ehret, D.J., Macfadden, B.J., Jones, D.S., DeVries, T.J., Foster, D.A., Salas-Gismondi, R. (2012). Origin of the white shark *Carcharodon* (Lamniformes: Lamnidae) based on recalibration of the Upper Neogene Pisco Formation of Peru. *Palaeontology*, 55, 1139-1153.

Ehret, D.J., MacFadden, B.J., Salas-Gismondi, R. (2009). Caught in the act: trophic interactions between a 4-million-year-old white shark (*Carcharodon*) and mysticete whale from Peru. *Palaios*, 24, 329-333.

Eckert, K.L., Wallace, B.P., Frazier, J.G., Eckert, S.A., Pritchard, P.C.H. (2012). Synopsis of the biological data on the leatherback sea turtle (*Dermochelys coriacea*). Jacksonville, U.S. Department of Interior, Fish and Wildlife Service.

Esperante, R., Brand, L.R., Chadwick, A.V., Poma, O. (2015). Taphonomy and paleoenvironmental conditions of deposition of fossil whales in the diatomaceous sediments of the Miocene/Pliocene Pisco Formation, southern Peru—a new Fossil-Lagerstätte. *Palaeogeography, Palaeoclimatology, Palaeoecology*, 417, 337-370.

Fallows, C., Gallagher, A.J., Hammerschlag, N. (2013). White sharks (*Carcharodon carcharias*) scavenging on whales and its potential role in further shaping the ecology of an apex predator. *PLOS ONE*, 8, article #e60797.

Fierstine, H.L. (2006). Fossil history of billfishes (Xiphioidei). *Bulletin of Marine Science*, 79, 433-453.

Föllmi, K.B., Grimm, K.A. (1990). Doomed pioneers: Gravity-flow deposition and bioturbation in marine dysaerobic environments. *Geology*, 18, 1069-1072.

Gariboldi, K., Gioncada, A., Bosio, G., Malinverno, E., Di Celma, C., Tinelli, C., Cantalamessa, G., Landini, W., Urbina, M., Bianucci, G. (2015). The dolomite nodules enclosing fossil marine vertebrates in the East Pisco Basin, Peru: field and petrographic insights into the Lagerstätte formation. *Palaeogeography, Palaeoclimatology, Palaeoecology*, 438, 81-95.

Gioncada, A., Collareta, A., Gariboldi, K., Lambert, O., Di Celma, C., Bonaccorsi, E., Urbina, M., Bianucci, G. (2016). Inside baleen: exceptional microstructure preservation in a late Miocene whale skeleton from Peru. *Geology*, 44, 839-842.

Gioncada, A., Gariboldi, K., Collareta, A., Di Celma, C., Bosio, G., Malinverno, E., Lambert, O.,

Pike, J., Urbina, M., Bianucci, G. (2018). Looking for the key to preservation of fossil marine vertebrates in the Pisco Formation of Peru: new insights from a small dolphin skeleton. *Andean Geology*, 45, in press.

Gioncada, A., Petrini, R., Bosio, G., Gariboldi, K., Collareta, A., Malinverno, E., Bonaccorsi, E., Di Celma, C., Pasero, M., Urbina, M., Bianucci, G. (2018). Insights into the diagenetic environment of fossil marine vertebrates of the Pisco Formation (late Miocene, Peru) from mineralogical and Sr-isotope data. *Journal of South American Earth Sciences*, 81, 141-152.

Hammer, Ø., Harper, D.A.T., Ryan, P. D. (2001). PAST: Paleontological statistics software package for education and data analysis. *Palaeontologia Electronica*, 4.1.4:1-9.

Hampel, A., Kukowski, N., Bialas, J., Heubscher, C., Heinbockel, R. (2004). Ridge subduction at an erosive margin: the collision zone of the Nazca Ridge in southern Peru. *Journal of Geophysical Research*, 109. article #B02101.

Hernández-Molina, F.J., Fernández-Salas, L.M., Lobo, F., Somoza, L., Díaz-del-Río, V., Alverinho Dias, J.M. (2000). The infralittoral prograding wedge: a new large-scale progradational sedimentary body in shallow marine environments. *Geo-Marine Letters*, 20, 109-117.

James, N.P. (1997). The cool-water carbonate depositional realm. In: James, N.P., Clarke, J.A.D. (Eds.), Cool-water Carbonates. *SEPM Special Publications*, 56, 1-20.

Jardas, I., Šantić, M., Armin, P. (2004). Diet composition of the eagle ray, *Myliobatis aquila* (Chondrichthyes: Myliobatidae), in the eastern Adriatic. *Cybium*, 28, 372-374.

Kellogg, R. (1927). *Kentriodon pernix*, a Miocene porpoise from Maryland. *Proceedings of the United States National Museum*, 69, 1-55.

Kellogg, R. (1932). A Miocene long-beaked porpoise from California. *Smithsonian Miscellaneous Collections*, 87: 1-11.

Kidwell, S.M. (1991). Condensed deposits in siliciclastic sequences: Expected and observed features. In: Einsele, G., Ricken,W., Seilacher, A. (Eds.), Cycles and events in stratigraphy.

Heidelberg, Springer-Verlag, 682-695.

Kidwell, S.M., Powars, D.S., Edwards, L.E., Vogt, P.R. (2015). Miocene stratigraphy and paleoenvironments of the Calvert Cliffs, Maryland. *Geological Society of America Field Guide*, 40, 231-279.

Kiel, S., Goedert, J.L., Kahl, W.-A., Rouse, G.W. (2010). Fossil traces of the bone-eating worm *Osedax* in early Oligocene whale bones. *PNAS*, 107, 8656-8659.

Kitchell, J.F., Martell, S.J., Walters, C.J., Jensen, O.P., Kaplan, I.C., Watters, J., Essington, T.E., Boggs, C.H. (2006). Billfishes in an ecosystem context. *Bulletin of Marine Science*, 79, 669-682.

Kulm, L.D., Resig, J.M., Thornburg, T.M., Schrader, H.J. (1982). Cenozoic structure, stratigraphy and tectonics of the central Peru forearc. In: Legget J.K. (Ed.), Trench and forearc geology: sedimentation and tectonics on modern and ancient plate margins. London, Blackwells, 151-169.

Lambert, O., Bianucci G., Muizon C de. (2017). Macroraptorial sperm whales (Cetacea, Odontoceti, Physeteroidea) from the Miocene of Peru. *Zoological Journal of the Linnean Society*, 179, 404-474.

Lambert, O., Bianucci, G., Urbina, M. (2014). *Huaridelphis raimondii*, a new early Miocene Squalodelphinidae (Cetacea, odontoceti) from the Chilcatay Formation, Peru. *Journal of Vertebrate Paleontology*, 34, 987-1004.

Lambert, O., Collareta, A., Landini, W., Post, K., Ramassamy, B., Di Celma, C., Urbina, M., Bianucci, G. (2015a). No deep diving: evidence of predation on epipelagic fish for a stem beaked whale from the late Miocene of Peru. *Proceedings of the Royal Society of London B*, 202, article #20151530.

Lambert, O., Gigase, P. (2007). A monodontid cetacean from the Early Pliocene of the North Sea. *Bulletin de l'Institut Royal des Sciences Naturelles de Belgique-Sciences de la Terre*, 77, 197-210.

Lambert, O., Martínez-Cáceres, M., Bianucci, G., Di Celma, C., Salas-Gismondi, R., Steurbaut, E.,

Urbina, M., Muizon, C. de (2017a). Earliest mysticete from the Late Eocene of Peru sheds new light on the origin of baleen whales. *Current Biology*, 27, 1535-1541.

Lambert, O., Muizon, C. de, Bianucci, G. (2015b). A new archaic homodont toothed cetacean (Mammalia, Cetacea, Odontoceti) from the early Miocene of Peru. *Geodiversitas*, 37, 79-108.

Lambert, O., Muizon, C. de, Malinverno, E., Celma, C. D., Urbina, M., Bianucci, G. (2018). A new odontocete (toothed cetacean) from the Early Miocene of Peru expands the morphological disparity of extinct heterodont dolphins. *Journal of Systematic Palaeontology*, 16(12), 981-1016.

Landini, W., Altamirano-Sierra, A., Collareta, A., Di Celma, C., Urbina, M., Bianucci, G. (2017a). The new Late Miocene chondrichthyan assemblage from Cerro Colorado (Pisco Formation, Peru). *South American Journal of Earth Sciences*, 73, 168-190.

Landini, W., Collareta, A., Pesci, F., Di Celma, C., Urbina, M., Bianucci, G. (2017b). A secondary nursery area for the copper shark *Carcharhinus brachyurus* from the late Miocene of Peru. *South American Journal of Earth Sciences*, 78, 164-174.

Landini, W., Collareta, A., Di Celma, C., Malinverno, E., Urbina, M., Bianucci, G. (2018). The early Miocene elasmobranch assemblage from Zamaca (Chilcatay Formation, Peru). *South American Journal of Earth Sciences*, in press, DOI: 10.1016/j.jsames.2018.08.004.

León, W., Aleman, A., Torres, V., Rosell, W., De la Cruz, O. (2008). Estratigrafía, sedimentología y evolución tectónica de la cuenca Pisco Oriental. *Boletín INGEMMET*, 27, 144 pp.

Long, D.J., Jones, R.E. (1996). White shark predation and scavenging on cetaceans in the eastern North Pacific Ocean. In: Klimley, A.P., Ainley, D.G. (Eds.), Great white sharks: the biology of *Carcharodon carcharias*. San Diego, Academic Press, 293-307.

Lucchi, F., Tranne, C.A., Rossi, P.L. (2010). Stratigraphic approach to geological mapping of the late Quaternary volcanic island of Lipari (Aeolian archipelago, southern Italy). *Geological Society of America Special Papers*, 464, 1-32.

McCurry, M.R., Evans, A.R., Fitzgerald, E.M.G., Adams, J.W., Clausen, P.D., McHenry, C.R.

(2017). The remarkable convergence of skull shape in crocodilians and toothed whales. *Proceedings of the Royal Society of London B*, 284, article #20162348.

Manojkumar, P.P., Pavithran, P.P. (2004). First record of snaggletooth shark, *Hemipristis elongatus* (Klunzinger, 1871) from Malabar Coast. *Marine Fisheries Information Service, Technical and Extension Series*, 180, 13-14.

Marocco, R., Muizon, C. de, (1988). Le Bassin Pisco, bassin cénozoïque d'avant arc de la côte du Pérou central: analyse géodynamique de son remplissage. *Géodynamique*, 3, 3-19.

Marx, F.G., Fordyce, R.E. (2015). Baleen boom and bust: a synthesis of mysticete phylogeny, diversity and disparity. *Royal Society Open Science*, 2, article #140434.

Marx, F.G., Uhen, M.D. (2010). Climate, critters, and cetaceans: Cenozoic drivers of the evolution of modern whales. *Science*, 327, 993-996.

Martínez-Cáceres, M., Lambert, O., Muizon, C. de (2017). The anatomy and phylogenetic affinities of *Cynthiacetus peruvianus*, a large *Dorudon*-like basilosaurid (Cetacea, Mammalia) from the late Eocene of Peru. *Geodiversitas*, 39, 7-163.

Massari, F., Chiocci, F. (2006). Biocalcarenite and mixed cool-water prograding bodies of the Mediterranean Pliocene and Pleistocene: architecture, depositional setting and forcing factors. In: Pedley, H.M., Carannante, G. (Eds.), Cool-water carbonates: depositional systems and palaeoenvironmental controls. *Geological Society, London, Special Publications*, 255, 95-120.

Massari, F., D'Alessandro, A. (2012) Facies partitioning and sequence stratigraphy of a mixed siliciclastic-carbonate ramp stack in the Gelasian of Sicily (S Italy): a potential model for icehouse, distally steepened heterozoan ramps. *Rivista Italiana di Paleontologia e Stratigrafia*, 118, 503-534.

Mitchell, N.C., Masselink, G., Huthnance, J.M., Fernández-Salas, L.M., Lobo, F.J. (2012) Depths of modern coastal sand clinoforms. *Journal of Sedimentary Research*, 82, 469-481.

Molina, J.M., Cazorla, A.L. (2015). Biology of *Myliobatis goodei* (Springer, 1939), a widely

distributed eagle ray, caught in northern Patagonia. *Journal of Sea Research*, 95, 106-114.

Noriega, J.I., Cione, A.L., Aceñolaza, F.G. (2007). Shark tooth marks on Miocene balaenopterid cetacean bones from Argentina. *Neues Jahrbuch für Geologie und Paläontologie-Abhandlungen*, 245, 185-192.

Norris, R.D, Kirtland Turner, S., Hull, P.M, Ridgwell, A. (2013). Marine ecosystem responses to Cenozoic global change. *Science*, 341, 492–498.

Peverell, S.C. (2009). Sawfish (Pristidae) of the Gulf of Carpentaria, Queensland, Australia. Unpublished MSc thesis, James Cook University (Australia), 147 pp.

Pickering, K.T., Hiscott, R.N., Hein, F.J. (1989). Deep-marine environments: clastic sedimentation and tectonics. London, Unwin Hyman.

Pimiento, C., MacFadden, B.J., Clements, C.F., Varela, S., Jaramillo, C., Velez-Juarbe, J., Silliman, B.R. (2016). Geographical distribution patterns of *Carcharocles megalodon* over time reveal clues about extinction mechanisms. *Journal of Biogeography*, 43, 1645-1655.

Pomar, L., Aurell, M., Bádenas, B., Morsilli, M., Al-Awwad, S.F. (2015) Depositional model for a prograding oolitic wedge, Upper Jurassic, Iberian basin. *Marine and Petroleum Geology*, 67, 556-582.

Pomar, L., Kendall, C. G. St. C. (2008). Carbonate platform architecture; a response to hydrodynamics and evolving ecology. In: Lukasik, J., Simo, T. (Eds.), Controls on carbonate platform and reef development. *SEPM Special Publication*, 89, 187-216.

Pomar, L., Tropeano, M. (2001) The calcarenite di Gravina Formation in Matera (southern Italy): new insights for coarse-grained, large scale, cross-bedded bodies encased in offshore deposits. *AAPG Bulletin*, 85, 661-689.

Pratt, H.L., Jr., Casey, J.G., Conklin, R.B. (1982). Observations on large white shark, *Carcharodon carcharias*, off Long Island, New York. *Fishery Bulletin*, 80, 153-156.

Purdy, R.W., Schneider, V.P., Applegate, S.P., Mclellan, J.H., Meyer, R.L., Slaughter, R. 2001.The

Neogene sharks, rays, and bony fishes from Lee Creek Mine, Aurora, North Carolina. In: Ray, C.E., Bohaska, D.J. (Eds.), Geology and paleontology of the Lee Creek Mine, North Carolina, III. *Smithsonian Contributions to Paleobiology*, 90, 71-202.

Pyenson, N.D., Irmis, R.B., Lipps, J.H., Barnes, L.G., Mitchell Jr, E.D., McLeod, S.A. (2009). Origin of a widespread marine bonebed deposited during the middle Miocene Climatic Optimum. *Geology*, 37, 519-522.

Raiswell, R., Berner, R.A. (1985). Pyrite formation in euxinic and semi-euxinic sediments. *American Journal of Science*, 285, 710-724.

Ramassamy, B., Lambert, O., Collareta, A., Urbina, M., Bianucci, G. (2018). Description of the skeleton of the fossil beaked whale *Messapicetus gregarius*, searching potential proxies for deep diving abilities. *Fossil Record*, 21, 11-32.

Reisdorf, A.G., Anderson, G.S., Bell, L.S., Klug, C., Schmid-Röhl, A., Röhl, H.J., Jung, M., Wuttke, M., Maisch, M.W., Benecke, M., Wyler, D., Bux, R., Fornaro, P., Wetzel, A. 2014. Reply to "Ichthyosaur embryos outside the mother body: not due to carcass explosion but to carcass implosion" by van Loon (2013). *Palaeobiodiversity and Palaeoenvironments*, 94, 487-494.

Rezende, G.A. de, Capitoli, R.R., Vooren, C.M. (2015). Dieta e morfologia da cabeça, boca e dentição de duas raias simpátricas, *Myliobatis goodei* e *M. ridens* (Batoidea: Myliobatiformes). *Boletim do Museu de Biologia Mello Leitão*, 37, 255-270.

Rivera, T.A., Storey, M., Zeeden, C., Hilgen, F.J., Kuiper, K. (2011). A refined astronomically calibrated $^{40}Ar/^{39}Ar$ age for Fish Canyon sanidine. *Earth and Planetary Science Letters*, 311, 420-426.

Rustichelli, A., Di Celma, C., Tondi, E., Baud, P., Vinciguerra, S. (2016a). Fibrous gypsum veins as diffuse features and within fault zones: the case study of the Pisco Basin (Ica desert, southern Peru). *Journal of the Geological Society*, 173, 405-418.

Rustichelli, A., Di Celma, C., Tondi, E., Bianucci, G. (2016b). Deformation within the Pisco basin

sedimentary record (southern Peru): Stratabound orthogonal vein sets and their impact on fault development. *Journal of South American Earth Sciences*, 65, 79-100.

Santini, F., Carnevale, G., Sorenson, L. (2013). First molecular scombrid timetree (Percomorpha: Scombridae) shows recent radiation of tunas following invasion of pelagic habitat. *Italian Journal of Zoology*, 80, 210-221.

Schäfer, W. (1972). Ecology and palaeoecology of marine environments. Chicago, University of Chicago Press.

Shimada, K., Chandler, R.E., Lam, O.L.T., Tanaka, T., Ward, D.J. (2017). A new elusive otodontid shark (Lamniformes: Otodontidae) from the lower Miocene, and comments on the taxonomy of otodontid genera, including the 'megatoothed'clade. *Historical Biology*, 29, 704-714.

Simpfendorfer, C.A., Burgess, G.H. (2009). *Carcharhinus leucas*. In: The IUCN Red List of Threatened Species 2013: e.T39372A10187195. http://www.iucnredlist.org, accessed on April 28, 2018.

Smile, M.J. (1991). Occurrence and feeding of three shark species, *Carcharhinus brachiurus*, *C. obscurus* and *Sphyrna zygaena*, on the Eastern Cape coast of South Africa. *South African Journal of Marine Science*, 11, 31-42.

Smith, C.R., Glover, A.G., Treude, T., Higgs, N.D., Amon, D.J. (2015). Whale-fall ecosystems: recent insights into ecology, paleoecology, and evolution. *Annual Review of Marine Science*, 7, 571-596.

Thornburg, T.M., Kulm, L.D. (1981). Sedimentary basins of the Peru continental margin: structure, stratigraphy, and Cenozoic tectonics from 6ºS to 16ºS latitude. In: Kulm, L.D., Dymond, J., Dasch, E.J., Hussong, D.M. (Eds.), Nazca plate: crustal formation and Andean convergence. *Geological Society of America Memoir*, 154, 393-422.

Travis, R.B., Gonzales, G., Pardo, A. (1976). Hydrocarbon potential of coastal basins of Peru. In: Halbouty, M., Maher, J., Lian, H.M. (Eds.), Circum-Pacific energy and mineral resources. *AAPG*

Memoir, 25, 331-338.

Uhen, M.D., Pyenson, N.D., DeVries, T.J., Urbina, M., Renne, P.R. (2011). New middle Eocene whales from the Pisco Basin of Peru. *Journal of Paleontology*, 85, 955-969.

Villa, I.M., Hermann, J., Müntener, O., Trommsdorff, V. (2000). $^{39}Ar/^{40}Ar$ dating of multiply zoned amphibole generations (Malenco, Italian Alps). *Contributions to Mineralogy and Petrology*, 140, 363-381.

Villa, I.M., Ruggieri, G., Puxeddu, M., Bertini, G. (2006). Geochronology and isotope transport systematics in a subsurface granite from the Larderello-Travale geothermal system (Italy). *Journal of Volcanology and Geothermal Research*, 152, 20-50.

Viveen, W., Schlunegger, F. (2018) Prolonged extension and subsidence of the Peruvian forearc during the Cenozoic. *Tectonophysics*, 730, 48-62.

von Huene, R., Lallemand, S. (1990). Tectonic erosion along the Japan and Peru convergent margins. *Geological Society of America Bulletin*, 102, 704-720.

Whitmore Jr, F.C., Kaltenbach, J.A. (2008). Neogene Cetacea of the Lee Creek Phosphate Mine, North Carolina. *Virginia Museum of Natural History Special Publication*, 14, 181-269.

Wilkin, R. T., Barnes, H. L., Brantley, S. L. (1996). The size distribution of framboidal pyrite in modern sediments: an indicator of redox conditions. *Geochimica et Cosmochimica Acta*, 60, 3897-3912.

Wood, R. C., Johnson-Gove, J., Gaffney, E. S., Maley, K. F. (1996). Evolution and phylogeny of the leatherback turtles (Dermochelyidae), with descriptions of new fossil taxa. *Chelonian Conservation and Biology*, 2, 266-286.

Wueringer, B.E., Squire, L., Collin, S.P. (2009). The biology of extinct and extant sawfish (Batoidea: Sclerorhynchidae and Pristidae). *Reviews in Fish Biology and Fisheries*, 19, 445-464.

Zúñiga-Rivero, F.J., Klein, G.D., Hay-Roe, H., Álvarez-Calderon, E. (2010). The hydrocarbon potential of Peru. Lima, BPZ Exploración & Producción S.R.L.

Table captions

Table 1. Overview of the lower Miocene marine vertebrate assemblage from *Ct1a* of the Chilcatay Formation exposed at Ullujaya, with a summary of the main taphonomic features of the fossil specimens. Isolated teeth and spines of Elasmobranchii and scales of Osteichthyes are not considered. Field numbers are after Di Celma et al. (2018). Abbreviation: Height abs = Height above the base of the section. Precise geographic coordinates of individual specimens are available on request from the corresponding author.

Table 2. Composition of the lower Miocene elasmobranch assemblage from *Ct1a* of the Chilcatay Formation exposed at Ullujaya.

Table 3. General prospect of the vertebrate specimens selected for the microscopic analyses, with a summary of the macro- and microscopic taphonomic features of the bones.

Table 4. Synoptic comparison of the main diversified lower Miocene cetacean assemblages worldwide. See main text for data sources.

Figure captions

Figure 1. A) Sketch map of the major sedimentary basins of coastal Peru showing the position of both the Outer Shelf Ridge and Upper Slope Ridge, redrawn and modified from Travis et al. (1976) and Thornburg & Kulm (1981). The red dashed rectangle outlines the location of the area shown in detail in Fig. 1B. B) Inferred palaeogeographic map of the EPB during the Miocene (redrawn and modified from Marocco and Muizon, 1988). This basin was a semi-enclosed, shallow littoral embayment partially separated from the open ocean by a chain of basement islands (the Gran Tablazo Archipelago of DeVries & Jud, 2018) of the emerging Outer Shelf Ridge. C) Close-up of the red dashed inset box in Fig. 1B showing the geographic location of the study area along the western side of the lower Ica valley.

Figure 2. A) Schematic stratigraphic column exhibiting the formational lithostratigraphy and the main component units of the Miocene portion of the basin fill of the EPB (not to scale). B) Simplified geological map showing the whole fossil vertebrate distribution for part of the Miocene succession exposed at Ullujaya (modified after Di Celma et al., 2018). C) Close- up of the black solid inset box in Fig. 2B further detailing the distribution of several tens of fossil vertebrate specimens at Ullujaya. D) Measured stratigraphic section. Note that, in the study area, all the allostratigraphic units dip gently towards NE. Clinoforms of *Ct1b* dip towards SW.

Figure 3. Field photographs. A) Depositional-dip oriented annotated panoramic view of the upper part of the Chilcatay Formation and the overlying Pisco Formation near Cerro Las Tres Piramides (geographic coordinates: 14°35'22"S, 75°38'20"W). The principal surfaces used to further subdivide the Chilcatay Formation into allomembers and the internal facies architecture

are indicated. Clinoforms of *Ct1b* prograde basinwards, showing truncated tops and typical downlapping basal contact onto subhorizontal and finer grained sediments of *Ct1a*. The Ct2 allomember rests on the CE0.2 unconformity and exhibits a pronounced retrogradational (fining-upward) facies trend. The Chilcatay and Pisco formations are separated by the PE0.0 unconformity. B) A 8-m-thick interval of siltstones and sandy siltstones that typify *Ct1a*. Note, just above the 1.8 m-long logging pole (encircled), the occurrence of a dark, granule-size conglomerate (black arrows) demarcated at its base by a conspicuous assemblage of moderate- to large-diameter *Thalassinoides* and *Gyrolithes* burrows (white arrows). These coarse grained beds indicate rare high-energy events that swept fragmented shells and small clasts into an otherwise quiescent environment. C-D) Close-up views of beds of shell debris and granule-size conglomerate intercalated within*Ct1a*. Note as subjacent silty strata are cut by a dense network of *Thalassinoides* and *Gyrolithes* burrows (white arrows) forming a *Glossifungites* suite. Burrows emanate from the base of the shell debris and granule-size conglomerate beds (dashed white line) and are infilled with overlying sediment.

Figure 4. Optical photos (A, B) and backscattered Scanning Electron Microscope (C, D) images of pyrite relics from the sediments of *Ct1a*. A) Rhombohedral crystals of dolomite associated with relics of pyrite framboids. B) Spherical relics of pyrite framboids. C) Rhombohedral crystals of dolomite. D) Detail of the framboidal texture of a pyrite relic.

Figure 5. Histograms of the size distribution of framboids in *Ct1a*, between 22 and 28.5 m abs. The number of pyrite framboids relics (N), the mean of framboid diameter, the Standard Deviation (SD) of the mean, and the percentage of framboids with a diameter greater than 10 μm are shown for each sample. Note the different distribution in the UL-D3 histogram with respect to the other samples.

Figure 6. A) Stratigraphic distribution of fossil vertebrates from *Ct1a* of the Chilcatay Formation exposed at Ullujaya. B) Quantitative composition of the fossil vertebrate assemblage of *Ct1a*, based on systematic surface prospecting (teeth and spines of Elasmobranchii are not considered). C) Quantitative composition of the fossil shark and ray assemblage from the *Ct1a* facies association, based on more than one thousand isolated teeth and spines.

Figure 7. Elasmobranch remains from *Ct1a* of the Chilcatay Formation exposed at Ullujaya. A) *Carcharocles chubutensis*. B) *Megalolamna paradoxodon*. C-D) *Cosmopolitodus hastalis*. E-F) I*surus oxyrinchus*. G) *Anotodus agassizii*. H) *Hemipristis serra*. I) *Alopias superciliosus*. J) *Physogaleus contortus*. K) *Galeocerdo aduncus*. L) *Carcharhinus* cf. *leucas*. M-N) *Carcharhinus brachyurus*. O-P) cf. *Myliobatis* sp. A-N) Lingual view. O) Occlusal view. P) Basal view.

Figure 8. Bedding view of fossil cetaceans from *Ct1a* of the Chilcatay Formation exposed at Ullujaya. A) Isolated cranium of *Kentriodon* sp. disposed ventral side-up position (field number: O7). B) Four associated and disarticulated vertebrae of aff. Odontoceti indet. (O57) and C) corresponding explanatory line drawing. D) Few associated and disarticulated bones (including mandibles and some vertebrae and ribs) of Odontoceti indet. (O29) and E) corresponding explanatory line drawing. F) Partial skeleton (including articulated vertebrae and disarticulated ribs and other fragmentary bones) of aff. Odontoceti indet. (O59) and G) corresponding explanatory line drawing. H) Fully disarticulated partial skeleton (including mandibles, humerus, ulna, vertebrae, and ribs.) of Squalodelphinidae indet. (O4) and G) corresponding explanatory line drawing. J) Seven articulated vertebrae of aff. Odontoceti indet. (O38) and K) Corresponding explanatory line drawing.

Figure 9. Fossil cetaceans (A-B, F-I) and tuna-like bony fish (C-E) from *Ct1a* of the Chilcatay Formation exposed at Ullujaya. Specimens depicted in panels F-I are exposed on vertical sections and exhibit evidence of partial sinking into the substratum. A) Disarticulated cranium, mandibles, and two ribs of an undescribed specimen of *Chilcacetus cavirhinus* (field number: O5; catalogue number: MUSM 2527) and B) corresponding explanatory line drawing. C) Fully articulated caudal fin (T2). D) Some associated and partially disarticulated vertebrae (T5). E) Few associated and partially disarticulated vertebrae and rays (T6). F) Three associated and disarticulated vertebrae of aff. Odontoceti indet. (field number: O40) with sunk transverse processes and G) corresponding explanatory line drawing. H) Partially articulated vertebral column of aff. Odontoceti indet. (O50) that moderately sank and I) corresponding explanatory line drawing. Red arrows indicate sinking of some portions of the bones.

Figure 10. Bubble plot of articulation versus completeness for the marine vertebrate assemblage from *Ct1a* of the Chilcatay Formation exposed at Ullujaya. Abbreviations: r^2 = Pearson's r-squared value; rs = Spearman rank-order correlation coefficient; T = intersect of the best-fit linear trend line with the completeness axis. For more details see chapter 3 of the present work and Beardmore et al. (2012).

Figure 11. Optical photos (A, B) and backscattered Scanning Electron Microscope images (C, F) of fossil marine mammal bones from *Ct1a* of the Chilcatay Formation exposed at Ullujaya. A) Detail of calcite cementing both the cancellous and the compact bone cavities of specimen O5; note that calcite started to grow from the surface of the bone trabecolae. B) Microborings on the bone surface of specimen O3. C) Transverse thin section in transmitted light of a rib from specimen O3; both cancellous and compact bone are visible. D) Reddish color of the bone surface of specimen O52 caused by the presence of Fe-oxyhydroxides. E) Cancellous bone of a

rib of specimen O5 showing an infill of sediment in some marrow cavities cemented by calcite. F) Microborings of the B-type (*sensu* Gariboldi et al., 2015) on the surface of a rib of specimen O3.

Figure 12. Evidences of fracturing on fossil cetaceans from *Ct1a* of the Chilcatay Formation exposed at Ullujaya. A) Cranium of *Kentriodon* sp. (MUSM 631) in lateral view, exhibiting a damaged posterior portion. B) The same in posterior view. C) Cranium of the holotype of of *Huaridelphis raimondii* (MUSM 1396) in lateral view, exhibiting weak fractures of the occipital shield and temporal region. D) The same in posterior view. Yellow arrows indicate the main direction of compression that originated the observed fracturing patterns.

Figure 13. Fossil cetacean bones displaying shark bite marks from *Ct1a* of the Chilcatay Formation exposed at Ullujaya. A-C and E-G) *Chilcacetus cavirhinus* (MUSM 2527). H-L). *Chilcacetus cavirhinus* (MUSM 1401). M-N) *Huaridelphis raimondii* (MUSM 1403). O) *Kentriodon* sp. A) Rib. B) Left humerus in medial view. C) The same in lateral view. D) Dried jaws of extant *Isurus oxyrinchus*. E) Sketch showing the shark gasping the flipper of the dolphin. F, G) Sketch showing the possible attack sequence, with the shark that bites the abdomen of the dolphin (F) before biting its flipper (G). H) Incomplete mandible in lateral view. I-N) Fragmentary ribs. O) Cranium in dorsal view.

Figure 14. Stylised reconstruction of the early Miocene marine vertebrate fauna of Ullujaya during deposition of *Ct1a*, highlighting the diversity of the assemblage described in the present work. Different species are shown as silhouettes, and are roughly to scale. Sediments belonging to *Ct1a* and *Ct1b* are cream and brown, respectively.

Figure 15. Diagram of framboid size distribution as a result of euxinic or oxic-dysoxic conditions. Data on modern euxinic and oxic-dysoxic environments are from Wilkin et al. (1996). Following the example of Agbi et al. (2015), these literature data are compared with our results. Samples from *Ct1a* provide evidence of the alternation of euxinic and oxic-dysoxic conditions at the seafloor.

Field Number	Height abs (m)	Determination	Preserved bones	*In situ*	Skull disposition	Skeletal completeness	Bone articulation	Marked recent erosion	Collected and kept at MUSM
		Cetacea							
O1	25.9	cf. *Diaphorocetus* sp.	cranium	yes	dorsal	0	0	-	-
O2	23.8	Physeteroidea indet.	cranium	yes	ventral	0	0	-	-
O3	15.0	*Huaridelphis raimondii*	partial skeleton including cranium, fragmentary mandibles, and some vertebrae and ribs	yes	-	1	0	-	yes
O4	27.9	Squalodelphinidae indet.	partial skeleton including mandibles, humeri, tympanic bulla, and some vertebrae and ribs	yes	-	2	0	-	in part
O5	9.7	*Chilcacetus cavirhinus*	partial skeleton including cranium, mandibles, humerus, some vertebrae and ribs	yes	dorsal	2	0	-	yes
O6	15.0	*Chilcacetus cavirhinus*	partial skeleton including cranium, mandibles and some vertebrae and ribs	yes	-	1	1	-	yes
O7	30.8	*Kentriodon* sp.	cranium	yes	ventral	0	0	-	-
O8	15.0	*Kentriodon* sp.	cranium with tympanic bulla	yes	-	0	0	-	-
O9	25.5	*Kentriodon* sp.	cranium	yes	-	0	0	-	yes
O10	25.5	*Kentriodon* sp.	cranium	yes	-	0	0	-	yes
O11	28.1	*Kentriodon* sp.	cranium	yes	dorsal	0	0	-	-
O12	17.4	*Kentriodon* sp.	cranium	yes	dorsal	0	0	-	-
O13	14.8	*Kentriodon* sp.	partial skeleton including cranium and some vertebrae and ribs	yes	-	1	1	-	-
O14	17.4	*Kentriodon* sp.	fragmentary cranium	yes	ventral	0	0	-	-
O15	23.3	*Kentriodon* sp.	cranium with ear bones	yes	ventral	0	0	-	-
O16	15.0	*Kentriodon* sp.	cranium, mandibles and portion of postcranial skeleton	yes	dorsal	1	0	-	yes
O17	15.0	*Kentriodon* sp.	cranium	yes	-	0	0	-	-
O18	24.1	*Kentriodon* sp.	fragmentary cranium	yes	-	0	0	-	-
O19	26.2	*Kentriodon* sp.	fragmentary cranium	yes	-	0	0	-	-
O20	27.7	Odontoceti indet.	fragments of humerus	yes	-	0	0	-	-
O21	29.2	Odontoceti indet.	fragmentary cranium	yes	ventral	0	0	present	-
O22	30.8	Odontoceti indet.	cranium	yes	dorsal	0	0	-	-
O23	30.3	Odontoceti indet.	fragmentary skeleton	yes	-	1	1	-	-
O24	29.2	Odontoceti indet.	rostrum, cervical vertebrae, and four thoracic vertebrae	yes	dorsal	1	3	-	-
O25	30.8	Odontoceti indet.	fragmentary cranium	yes	-	0	0	-	-
O26	25.9	Odontoceti indet.	fragmentary cranium	yes	-	0	0	-	-
O27	15.0	Odontoceti indet.	skull	yes	ventral	0	0	-	-
O28	29.2	Odontoceti indet.	fragmentary rostrum	yes	dorsal	0	0	present	-
O29	15.0	Odontoceti indet.	Mandible, vertebrae and ribs	yes	-	1	0	-	-
O30	17.4	Odontoceti indet.	fragmentary cranium	yes	-	0	0	present	-
O31	19.6	Odontoceti indet.	mandible fragment, thoracic vertebrae, ribs, scapula	yes	-	1	1	present	-
O32	13.9	Odontoceti indet.	rostrum fragment	yes	ventral	0	0	present	-
O33	21.7	Odontoceti indet.	fragments of cranium	yes	-	0	0	-	-

O34	16.4	Odontoceti indet.	cranium and ribs	yes	-	1	0	-	-
O35	21.7	Odontoceti indet.	cranium	yes	dorsal	0	0	present	-
O36	25.8	Odontoceti indet.	incomplete atlas and axis	no	-	-	-	-	-
O37	25.5	aff. Odontoceti indet.	caudal vertebrae	no	-	-	-	-	-
O38	28.1	aff. Odontoceti indet.	seven vertebrae	yes	-	1	4	-	-
O39	27.7	aff. Odontoceti indet.	fragments of vertebrae	no	-	-	-	-	-
O40	27.9	aff. Odontoceti indet.	lumbar and caudal vertebrae	yes	-	1	0	-	-
O41	26.2	aff. Odontoceti indet.	lumbar and caudal vertebrae	yes	-	1	0	-	-
O42	25.5	aff. Odontoceti indet.	lumbar and caudal vertebrae	no	-	-	-	-	-
O43	14.8	aff. Odontoceti indet.	fragmentary vertebrae	no	-	-	-	-	-
O44	14.2	aff. Odontoceti indet.	fragmentary vertebrae and ribs	yes	-	1	0	-	-
O45	14.2	aff. Odontoceti indet.	vertebrae (including atlas and axis) and ribs	yes	-	1	0	-	-
O46	14.8	aff. Odontoceti indet.	caudal vertebrae	no	-	-	-	-	-
O47	14.8	aff. Odontoceti indet.	vertebrae and ribs	no	-	-	-	-	-
O48	17.4	aff. Odontoceti indet.	vertebrae and ribs	yes	-	1	0	-	-
O49	17.4	aff. Odontoceti indet.	eight vertebrae	yes	-	1	2	present	-
O50	14.8	aff. Odontoceti indet.	thoracic vertebrae	yes	-	1	2	-	-
O51	24.7	aff. Odontoceti indet.	vertebrae and ribs	yes	-	1	2	-	-
O52	25.9	aff. Odontoceti indet.	fragmentary vertebrae	no	-	-	-	present	-
O53	27.4	aff. Odontoceti indet.	fragmentary vertebrae	no	-	-	-	present	-
O54	21.1	aff. Odontoceti indet.	fragmentary vertebrae	no	-	-	-	present	-
O55	14.2	aff. Odontoceti indet.	fragmentary vertebrae	no	-	-	-	present	-
O56	27.9	aff. Odontoceti indet.	cervical and thoracic vertebre	yes	-	1	2	-	-
O57	26.2	aff. Odontoceti indet.	lumbar to caudal vertebrae	yes	-	1	0	-	-
O58	33.5	aff. Odontoceti indet.	fragmentary vertebrae	no	-	-	-	present	-
O59	14.2	Odontoceti indet.	thoracic vertebrae and ribs	yes	-	1	2	-	-
O60	25.9	aff. Odontoceti indet.	vertebrae and ribs	yes	-	1	2	-	-
O61	25.9	aff. Odontoceti indet.	vertebrae and ribs	yes	-	1	0	-	-
O62	25.9	aff. Odontoceti indet.	lumbar vertebrae and ribs	yes	-	1	0	-	-
O63	16.4	aff. Odontoceti indet.	rib	yes	-	0	0	-	-
O64	26.2	aff. Odontoceti indet.	axis, thoracic vertebra and rib fragments	yes	-	1	0	-	-
O65	26.4	aff. Odontoceti indet.	fragmentary vertebrae	no	-	-	-	present	-
		Testudines							
R1	14.8	Testudines indet.	fragments of carapax and partial forelimb	yes	-	1	0	-	-
		Osteichthyes							
T1	28.1	aff. *Thunnus* sp.	skull bone (dentary)	yes	-	0	0	-	-
T2	29.2	aff. *Thunnus* sp.	caudal fin	yes	-	0	4	-	-
T3	26.4	aff. *Thunnus* sp.	fragment of skull bone (dentary)	yes	-	0	0	-	-
T4	14.8	aff. *Thunnus* sp.	vertebrae	yes	-	1	14	-	-

T5	14.2	aff. *Thunnus* sp.	thirteen vertebrae	yes	-	1	2	-	-
T6	14.2	aff. *Thunnus* sp.	seven vertebrae and rays	yes	-	1	2	-	-
T7	25.5	aff. *Thunnus* sp.	partial skeleton	yes	-	1	2	-	-
T8	25.2	aff. *Thunnus* sp.	vertebrae	yes	-	1	2	-	-
T9	25.5	aff. *Makaira* sp.	vertebrae, skull bones, and other skeletal elements	yes	-	2	2	-	-
T10	18.2	Osteichthyes indet.	cranium	yes	dorsal	0	0	-	-

Table 1

Table 2

Order	Family or Superfamily	Genus et species	Number of specimens
Lamniformes	Otodontidae	*Carcharias* sp.	2
	Alopiidae	*Alopias superciliosus*	5
		Anotodus agassizii	16
	Otodontidae	*Megalolamna paradoxodon*	1
		Carcharocles chubutensis	30
	Lamnidae	*Isurus oxyrinchus*	88
		Cosmopolitodus hastalis	242
Carcharhiniformes	Hemigaleidae	*Hemipristis serra*	10
	Carcharhinidae	*Physogaleus contortus*	48
		Galeocerdo aduncus	20
		Negaprion brevirostris	2
		Carcharhinus brachyurus	539
		Carcharhinus cf. *leucas*	2
	Sphyrnidae	*Sphyrna zygaena*	1
Myliobatiformes	Myliobatoidea	Myliobatoidea indet.	82
Rhinopristiformes	Pristidae	*Anoxypristis* sp.	2
			1090

Number	Height abs (m)	Determination	Analysed bone elements	Bone colour	Bone surface	Bone permineralization
O3	15.0	*Huaridelphis raimondii*	rib	reddish	partially dissolved, with borings	minor, Fe-oxides/hydroxides
O5	9.7	*Chilcacetus cavirhinus*	ribs	white to brownish	intact, no borings	high, calcite and dolomite
O16	15.0	*Kentriodon* sp.	rib	pinkish	intact, no borings	-
O29	15.0	Odontoceti indet.	bone fragment	reddish	partially dissolved, with borings	moderate, Ca-Mg carbonates
O41	26.2	aff. Odontoceti indet.	vertebra	white	worn out[(1)]	moderate, Ca-Mg carbonates
O52	25.9	aff. Odontoceti indet.	vertebra	reddish to black	worn out[(1)]	moderate, Ca-Mg carbonates
O53	27.4	aff. Odontoceti indet.	vertebra	brownish	worn out[(1)]	minor, Ca-phosphate and Fe- oxides/hydroxides

[(1)] the presence/absence of borings cannot be assessed due to the lack of bone surface.

Table 3

	Ullujaya locality, Chilcatay Fm (Peru) lower Burdigalian	**Arenarie di Belluno (Italy)** upper Aquitanian to lower Burdigalian	**Monte León Fm (Argentina)** Aquitanian	**Gaiman Fm (Argentina)** lower Burdigalian	**Pyramid Hill Sand Member, Jewett Sand Fm (California, USA)** Aquitanian	**Lower part Calvert Fm and Pungo River Fm (Delaware, Maryland, North Carolina, Virginia, USA)**
Odontoceti						
Physeteroidea						
Physeteridae	cf. *Diaphorocetus* sp.		*Diaphorocetus poucheti*	*Idiorophus patagonicus*		*Orycterocetus crocodilinus*
Physeteroidea indet.		*'Scaldicetus' bellunensis*				
Platanistoidea						
Allodelphinidae					*Allodelphis pratti*	
Dalpiazinidae		*Dalpiazina ombonii*				
Platanistidae						*Araeodelphis natator* *Zarhachis flagellator*
Prosqualodontidae				*Prosqualodon australis*		
Squalodelphinidae	*Notocetus vanbenedeni* *Huaridelphis raimondii*	*Squalodelphis fabianii*	*Notocetus vanbenedeni*			*Phocageneus venustus* Squalodelphinidae indet.
Squalodontidae		*Squalodon bariensis* *Squalodon bellunensis* *Squalodon peregrinus*		*Phoberodon arctirostris*		*Squalodon calvertensis* *Squalodon whitmorei*
Incertae sedis				*Aondelphis talen*		
Eurhinodelphinoidea						
Eurhinodelphinidae		*Mycteriacetus bellunensis* *Ziphiodelphis abeli* *Z. sigmoideus*		Eurhinodelphinidae indet.		*Schizodelphis morckhoviensis* *Xiphiacetus bossi*
Eoplatanistidae		*Eoplatanista italica* *E. gresalensis*				
Eurhinodelphinoid-like						
Incertae sedis	*Chilcacetus cavirhinus*			*Argyrocetus patagonicus*	*"Argyrocetus" bakersfieldensis* *"Argyrocetus" joaquinensis* *Macrodelphinus kelloggi* *Miodelphis californicus*	
Delphinida						
Kentriodontidae	*Kentriodon* sp.		*Kentriodon* sp.	*Kentriodon* sp.		*Kentriodon pernix* *Delphinodon dividum*
Mysticeti						
Balaenidae				*Morenocetus parvus*		

Cetotheriidae s.l.	*Aglaocetus moreni*	*Parietobalaena palmeri*

Table 4

Highlights for

Taphonomy and palaeoecology of the lower Miocene marine vertebrate assemblage of Ullujaya (Chilcatay Formation, East Pisco Basin, southern Peru)

by Giovanni Bianucci et alii.

- Early Miocene is an important but still poorly known phase in the evolutionary history of marine vertebrates.
- We report sedimentological, taphonomic and palaeaoecological observations on a conspicuous, newly discovered Burdigalian marine vertebrate assemblage from Peru consisting of sharks, rays, toothed whales, bony fish, and turtles.
- Vertebrates inhabited a 30-40 m deep, warm-temperate, semi-protected offshore setting.
- Their carcasses suffered prolonged flotation causing biogenic and physical processes of partial destruction.
- Preservation of vertebrates was favoured by the oxygen-deficient bottom conditions inhibiting the action of benthic macro-scavengers.

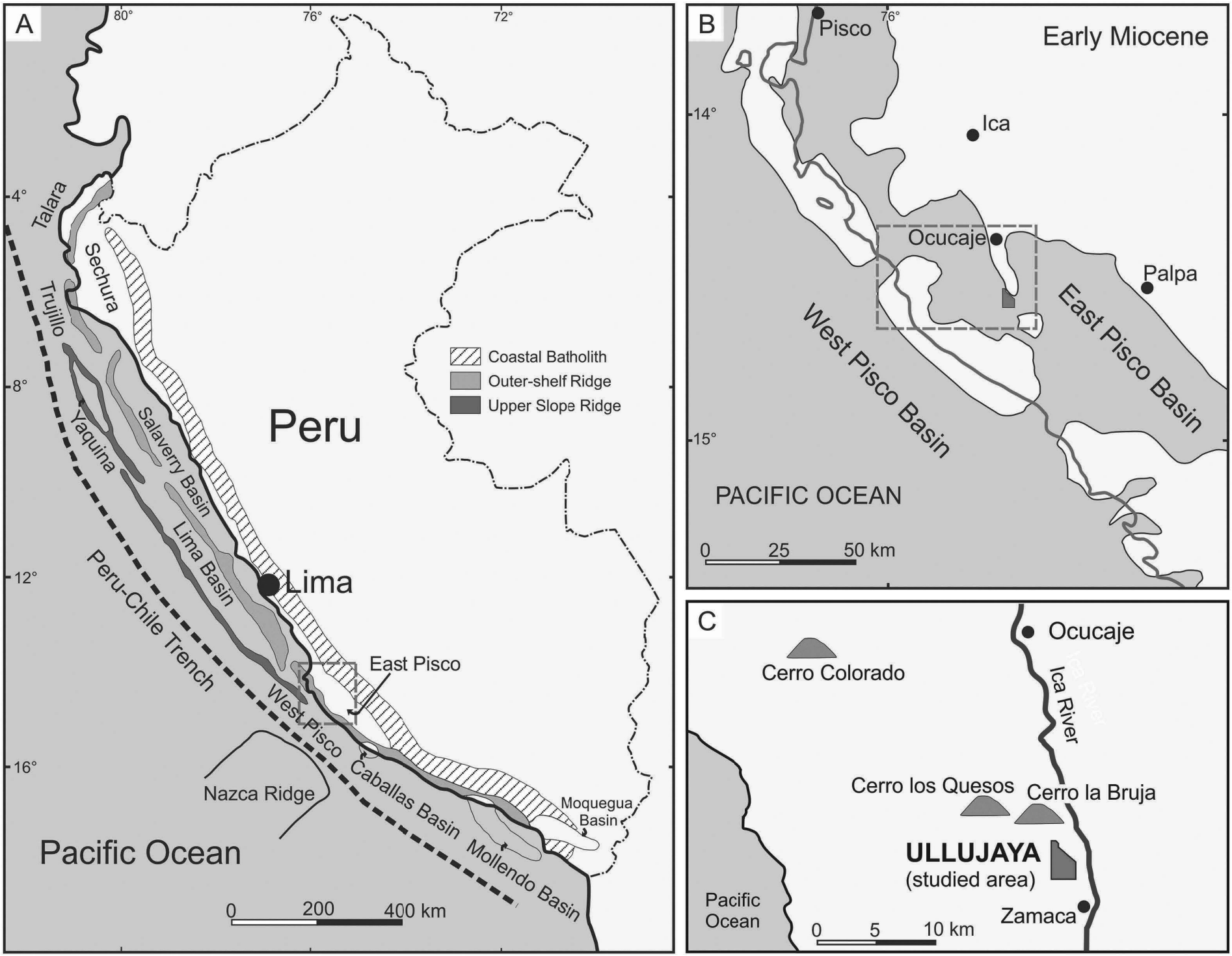
A
80°
76°
72°
4°
8°
12°
16°
Talara
Sechura
Trujillo
Yaquina
Salaverry Basin
Lima Basin
Peru-Chile Trench
Nazca Ridge
West Pisco
Caballas Basin
Mollendo Basin
Moquegua Basin
East Pisco
Lima
Peru
Pacific Ocean
Coastal Batholith
Outer-shelf Ridge
Upper Slope Ridge
0 200 400 km
B
Early Miocene
Pisco
Ica
Ocucaje
Palpa
West Pisco Basin
East Pisco Basin
PACIFIC OCEAN
14°
15°
0 25 50 km
C
Ocucaje
Cerro Colorado
Ica River
Cerro los Quesos
Cerro la Bruja
ULLUJAYA
(studied area)
Pacific Ocean
Zamaca
0 5 10 km

Figure 1

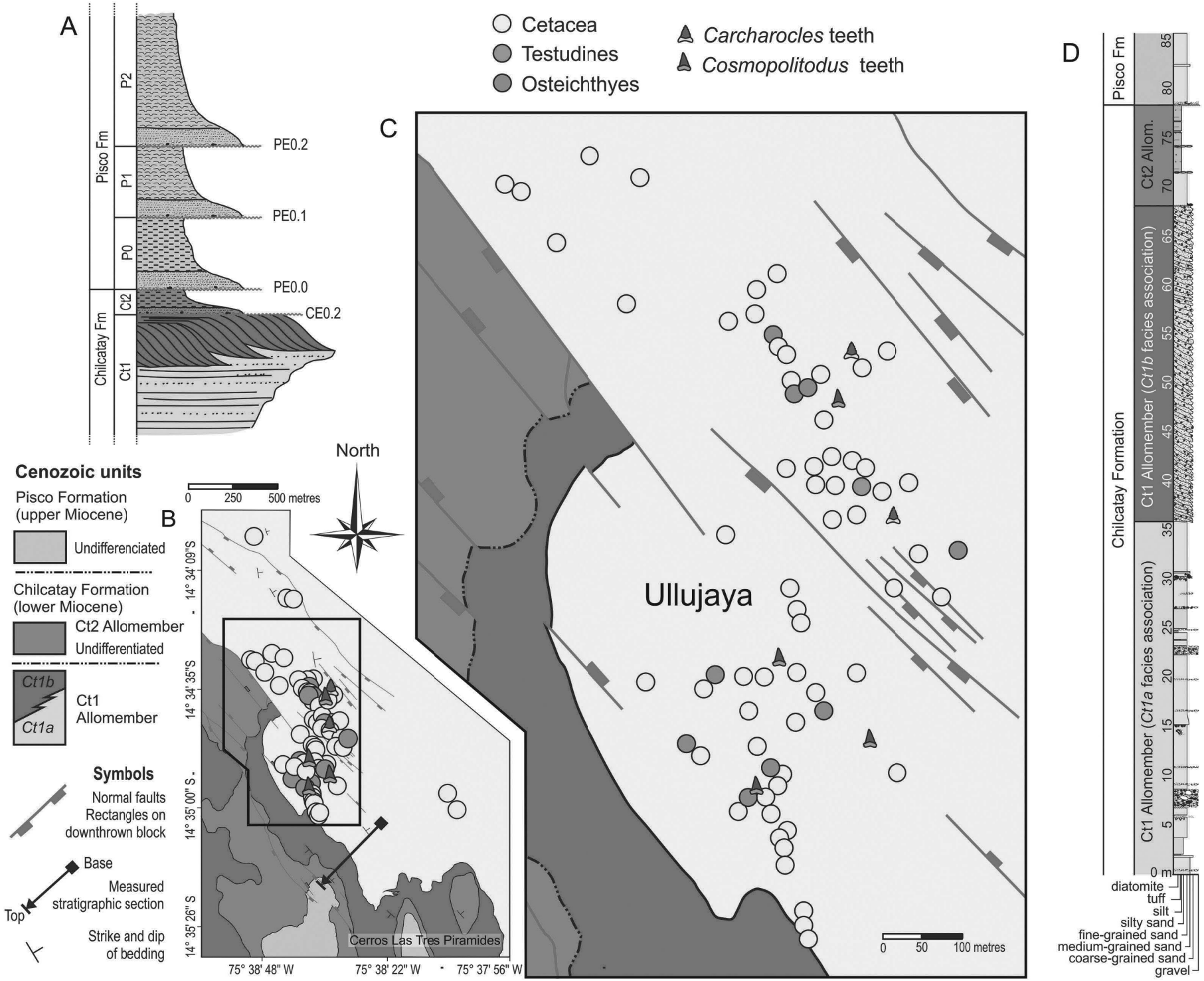
A
Pisco Fm
Chilcatay Fm
P2
P1
P0
Ct2
Ct1
PE0.2
PE0.1
PE0.0
CE0.2
Cetacea
Testudines
Osteichthyes
Carcharocles teeth
Cosmopolitodus teeth
C
Ullujaya
0 50 100 metres
D
Pisco Fm
Chilcatay Formation
Ct2 Allom.
Ct1 Allomember (Ct1b facies association)
Ct1 Allomember (Ct1a facies association)
0 m
diatomite
tuff
silt
silty sand
fine-grained sand
medium-grained sand
coarse-grained sand
gravel
Cenozoic units
Pisco Formation
(upper Miocene)
Undifferenciated
Chilcatay Formation
(lower Miocene)
Ct2 Allomember
Undifferentiated
Ct1b
Ct1a
Ct1
Allomember
Symbols
Normal faults
Rectangles on
downthrown block
Base
Top
Measured
stratigraphic section
Strike and dip
of bedding
B
North
0 250 500 metres
14° 34' 09" S
14° 34' 35" S
14° 35' 00" S
14° 35' 26" S
75° 38' 48" W
75° 38' 22" W
75° 37' 56" W
Cerros Las Tres Piramides

Figure 2

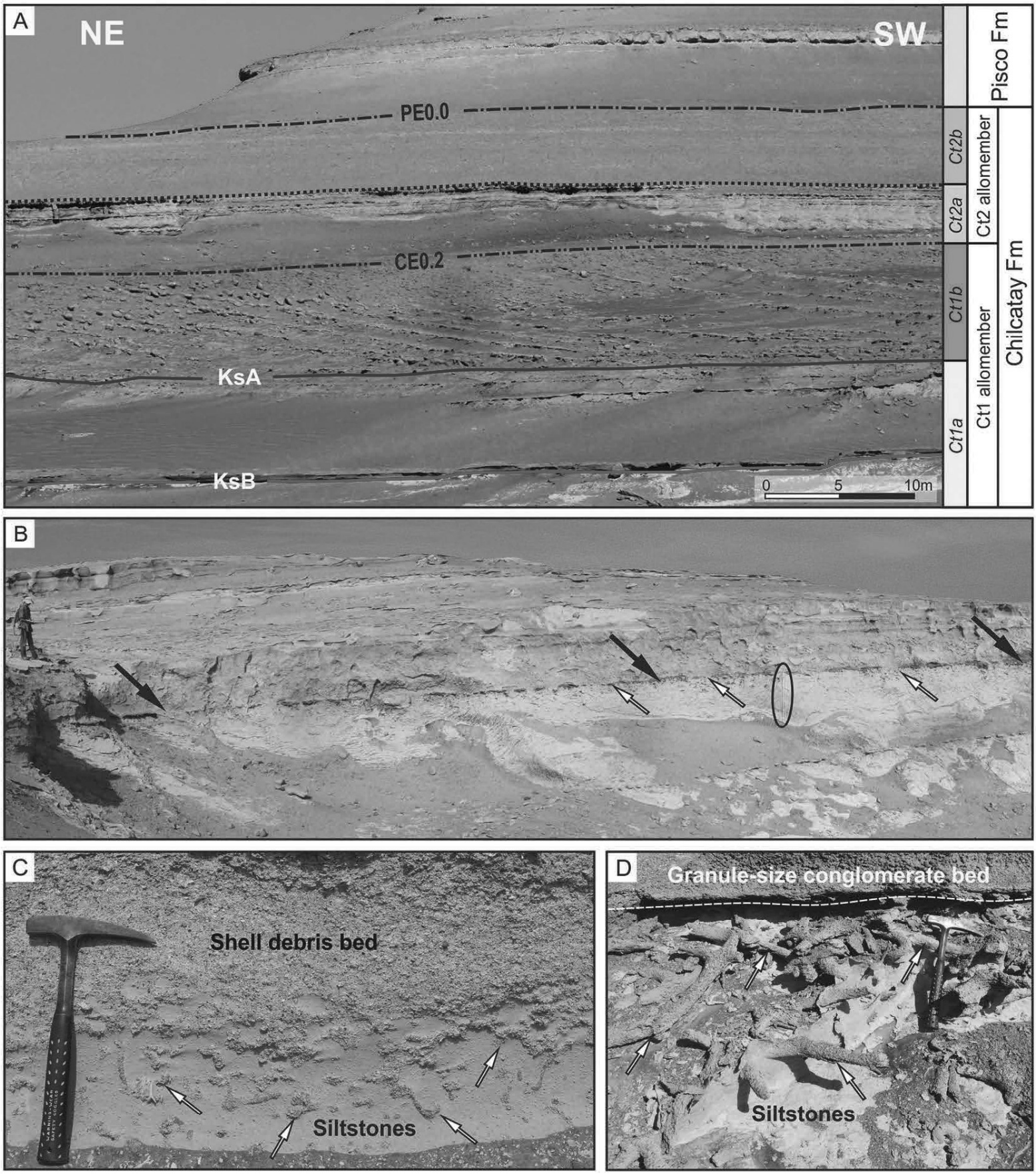
A
NE
SW
PE0.0
CE0.2
KsA
KsB
0
5
10m
Ct1a
Ct1b
Ct2a
Ct2b
Ct1 allomember
Ct2 allomember
Chilcatay Fm
Pisco Fm
B
C
Shell debris bed
Siltstones
D
Granule-size conglomerate bed
Siltstones

Figure 3

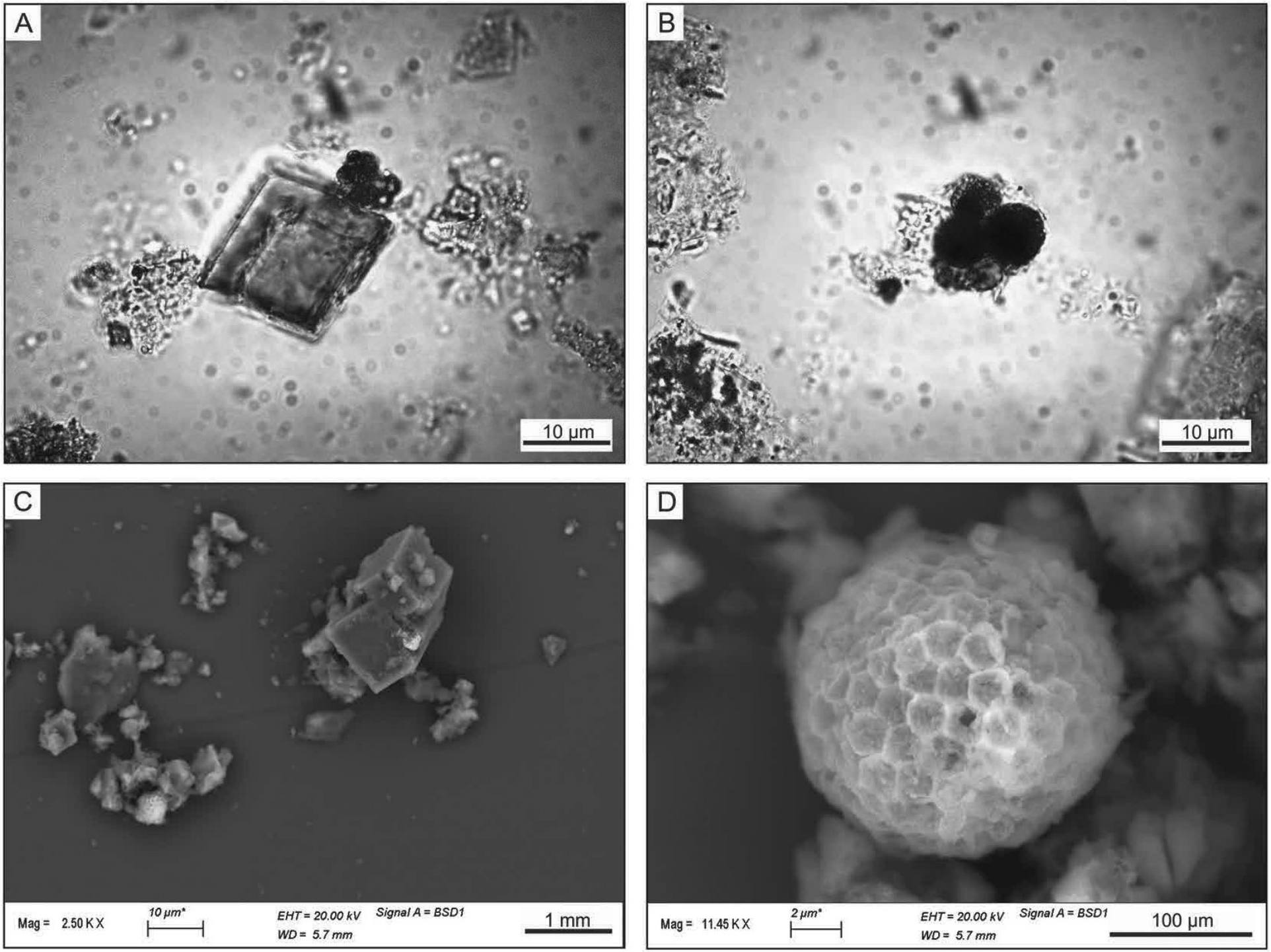
A
10 µm
B
10 µm
C
Mag = 2.50 K X
10 µm*
EHT = 20.00 kV
WD = 5.7 mm
Signal A = BSD1
1 mm
D
Mag = 11.45 K X
2 µm*
EHT = 20.00 kV
WD = 5.7 mm
Signal A = BSD1
100 µm

Figure 4

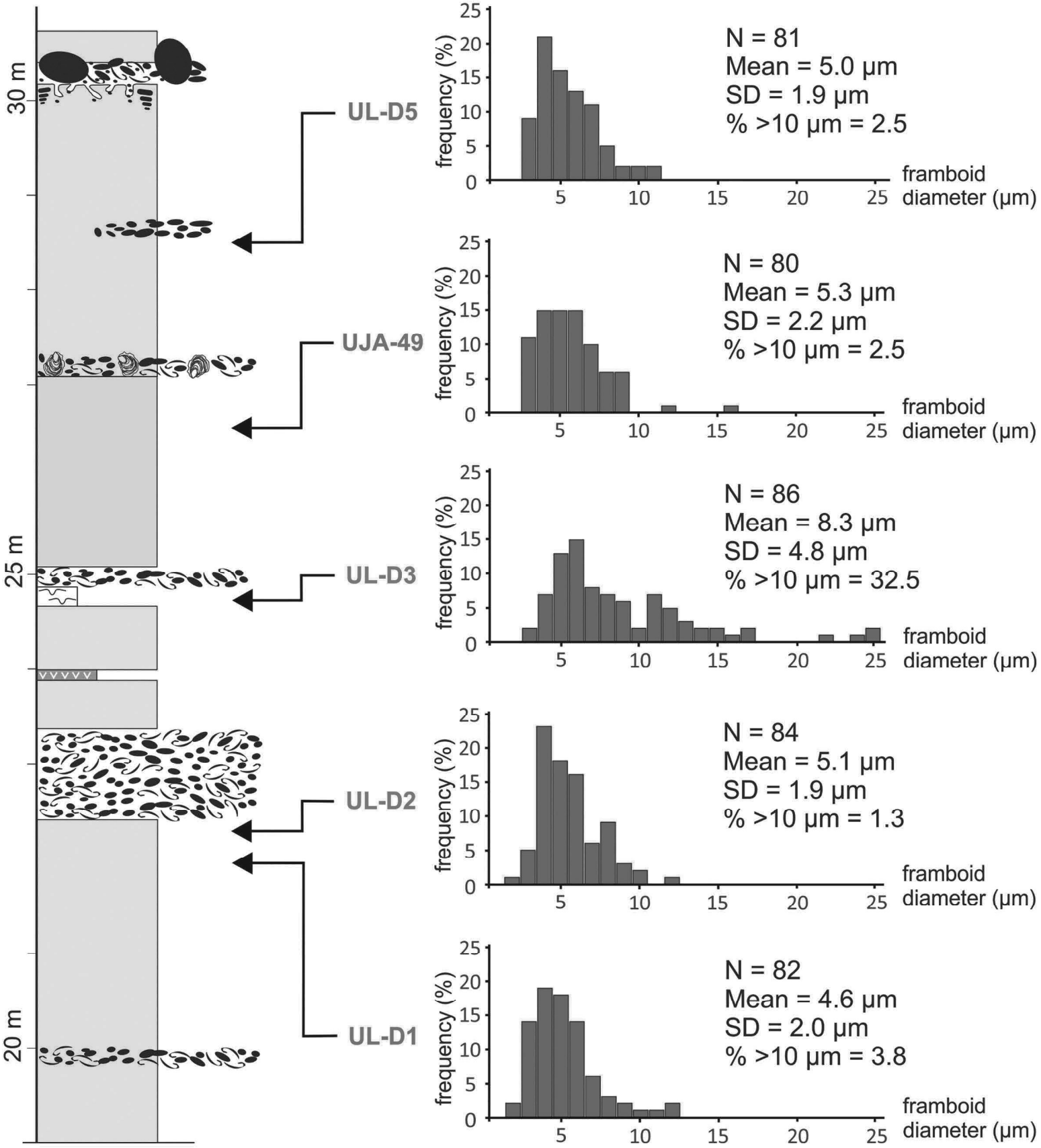
30 m
25 m
20 m
UL-D5
UJA-49
UL-D3
UL-D2
UL-D1
frequency (%)
framboid diameter (µm)
N = 81
Mean = 5.0 µm
SD = 1.9 µm
% >10 µm = 2.5
N = 80
Mean = 5.3 µm
SD = 2.2 µm
% >10 µm = 2.5
N = 86
Mean = 8.3 µm
SD = 4.8 µm
% >10 µm = 32.5
N = 84
Mean = 5.1 µm
SD = 1.9 µm
% >10 µm = 1.3
N = 82
Mean = 4.6 µm
SD = 2.0 µm
% >10 µm = 3.8

Figure 5

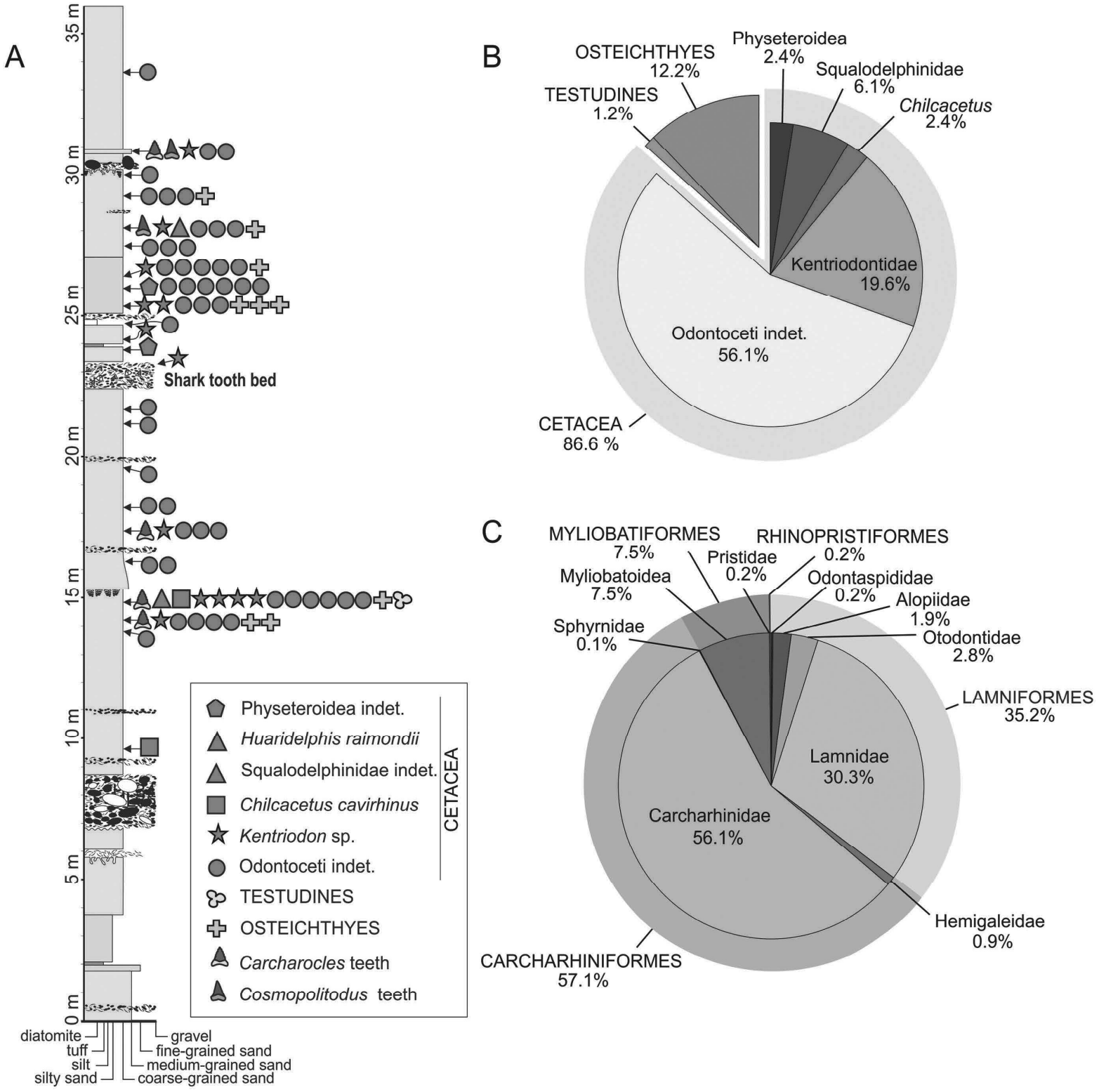
A
35 m
30 m
25 m
20 m
15 m
10 m
5 m
0 m
Shark tooth bed
Physeteroidea indet.
Huaridelphis raimondii
Squalodelphinidae indet.
Chilcacetus cavirhinus
Kentriodon sp.
Odontoceti indet.
TESTUDINES
OSTEICHTHYES
Carcharocles teeth
Cosmopolitodus teeth
CETACEA
diatomite
tuff
silt
silty sand
gravel
fine-grained sand
medium-grained sand
coarse-grained sand
B
OSTEICHTHYES 12.2%
Physeteroidea 2.4%
Squalodelphinidae 6.1%
TESTUDINES 1.2%
Chilcacetus 2.4%
Kentriodontidae 19.6%
Odontoceti indet. 56.1%
CETACEA 86.6 %
C
MYLIOBATIFORMES 7.5%
RHINOPRISTIFORMES 0.2%
Pristidae 0.2%
Myliobatoidea 7.5%
Odontaspididae 0.2%
Alopiidae 1.9%
Sphyrnidae 0.1%
Otodontidae 2.8%
LAMNIFORMES 35.2%
Lamnidae 30.3%
Carcharhinidae 56.1%
Hemigaleidae 0.9%
CARCHARHINIFORMES 57.1%

Figure 6

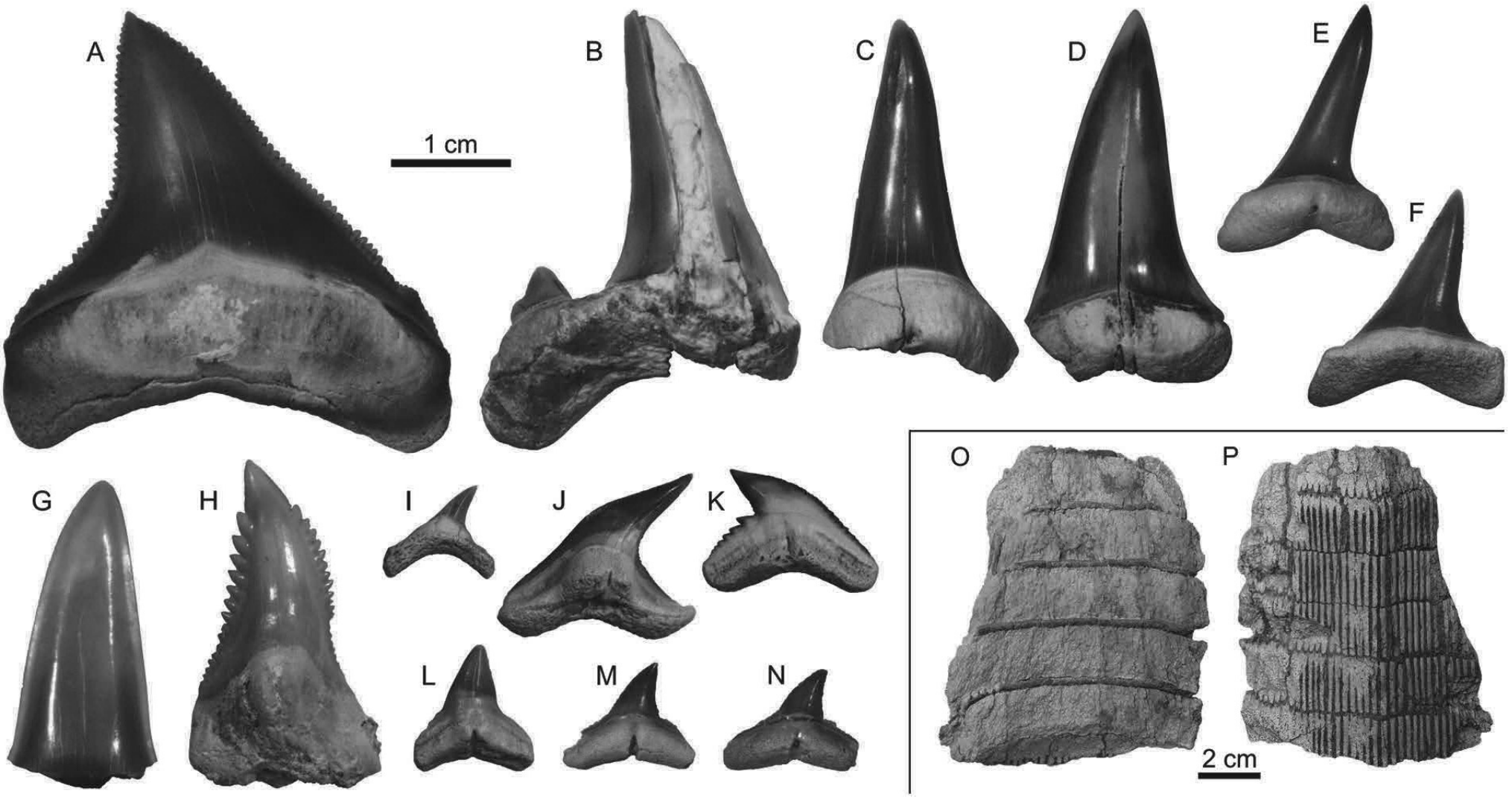

Figure 7

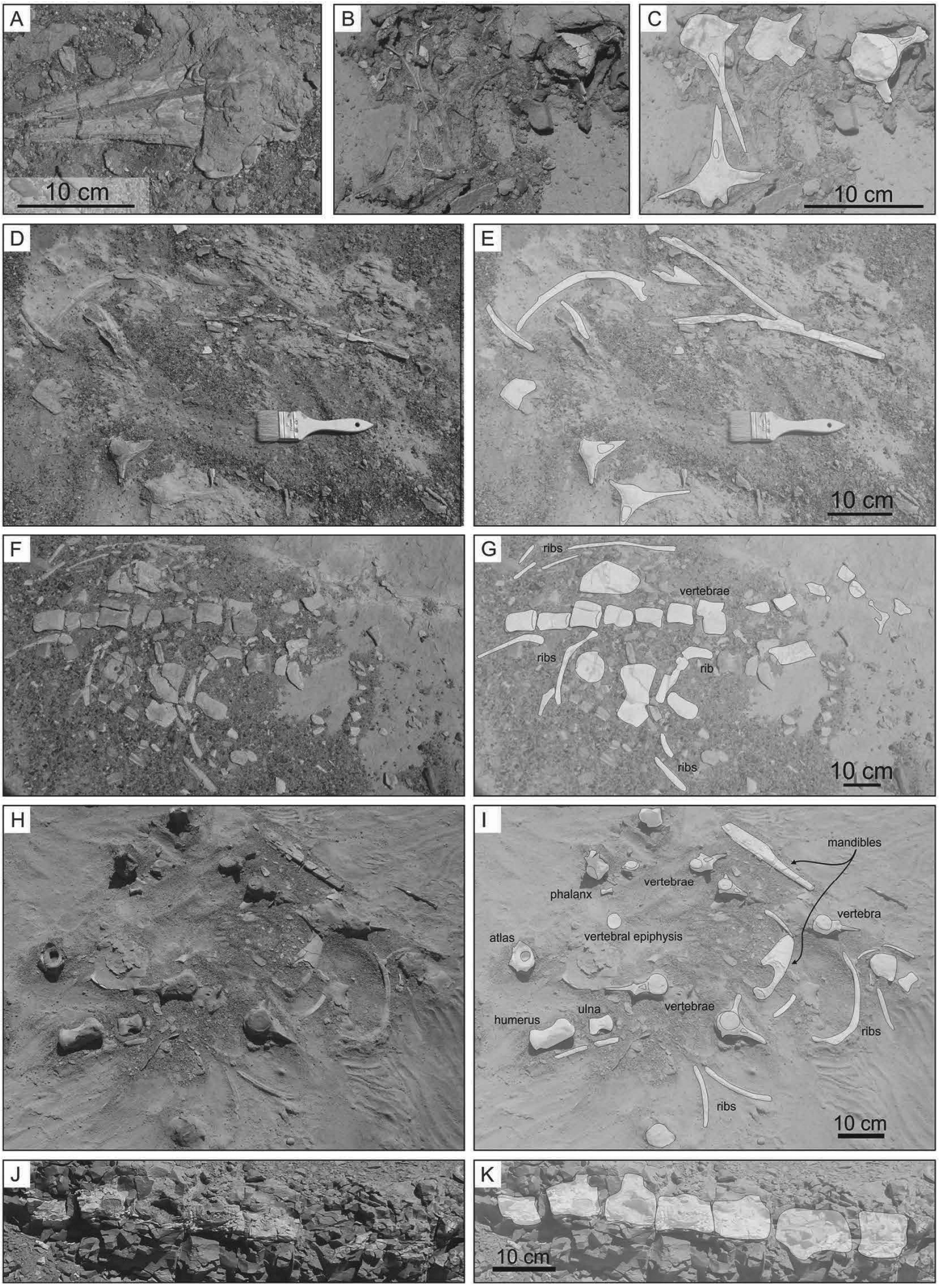
A
10 cm
B
C
10 cm
D
E
10 cm
F
G
ribs
vertebrae
ribs
rib
ribs
10 cm
H
I
mandibles
phalanx
vertebrae
vertebra
atlas
vertebral epiphysis
ulna
vertebrae
humerus
ribs
ribs
10 cm
J
K
10 cm

Figure 8

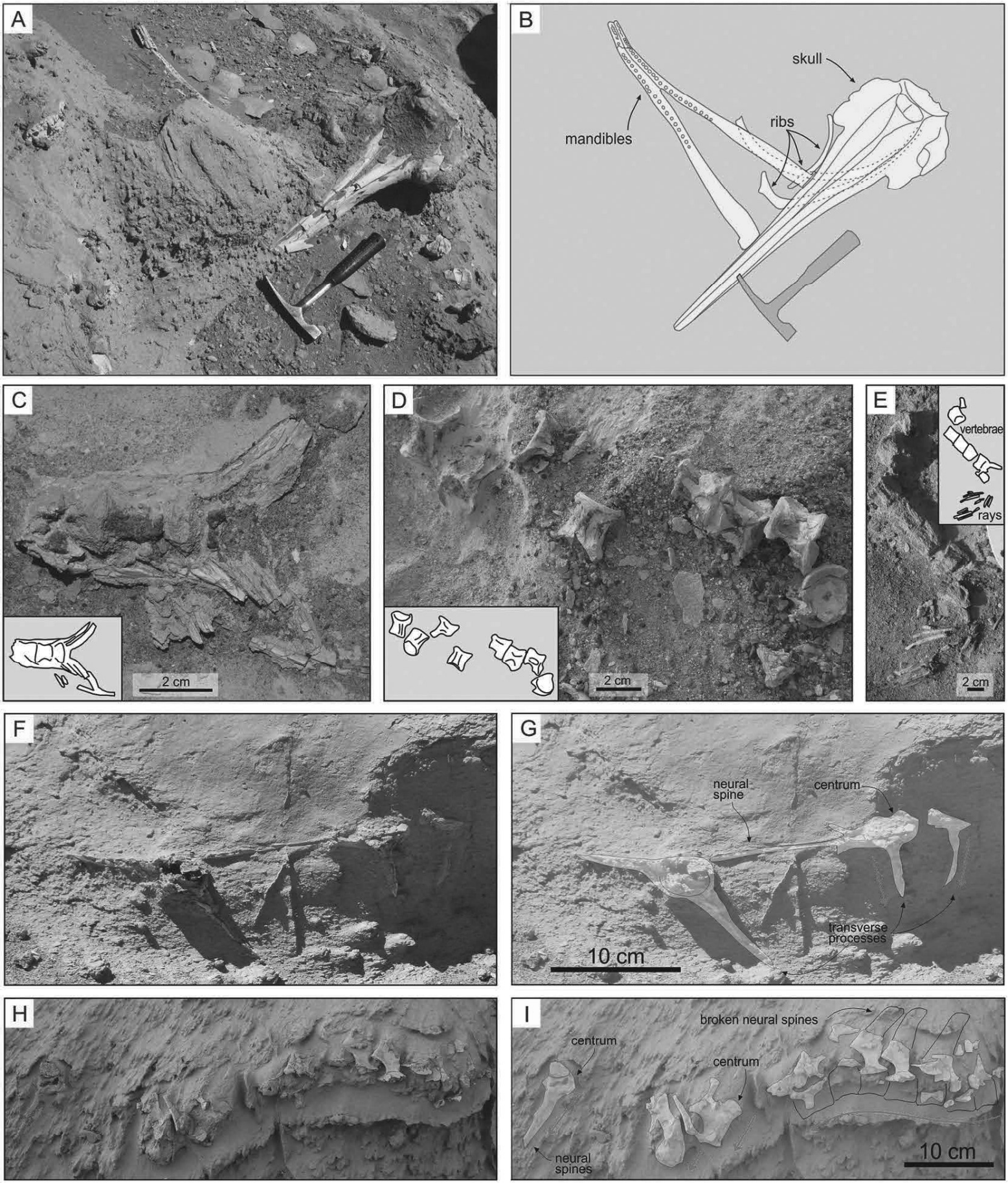
A
B
skull
ribs
mandibles
C
2 cm
D
2 cm
E
vertebrae
rays
2 cm
F
G
neural spine
centrum
transverse processes
10 cm
H
I
broken neural spines
centrum
centrum
neural spines
10 cm

Figure 9

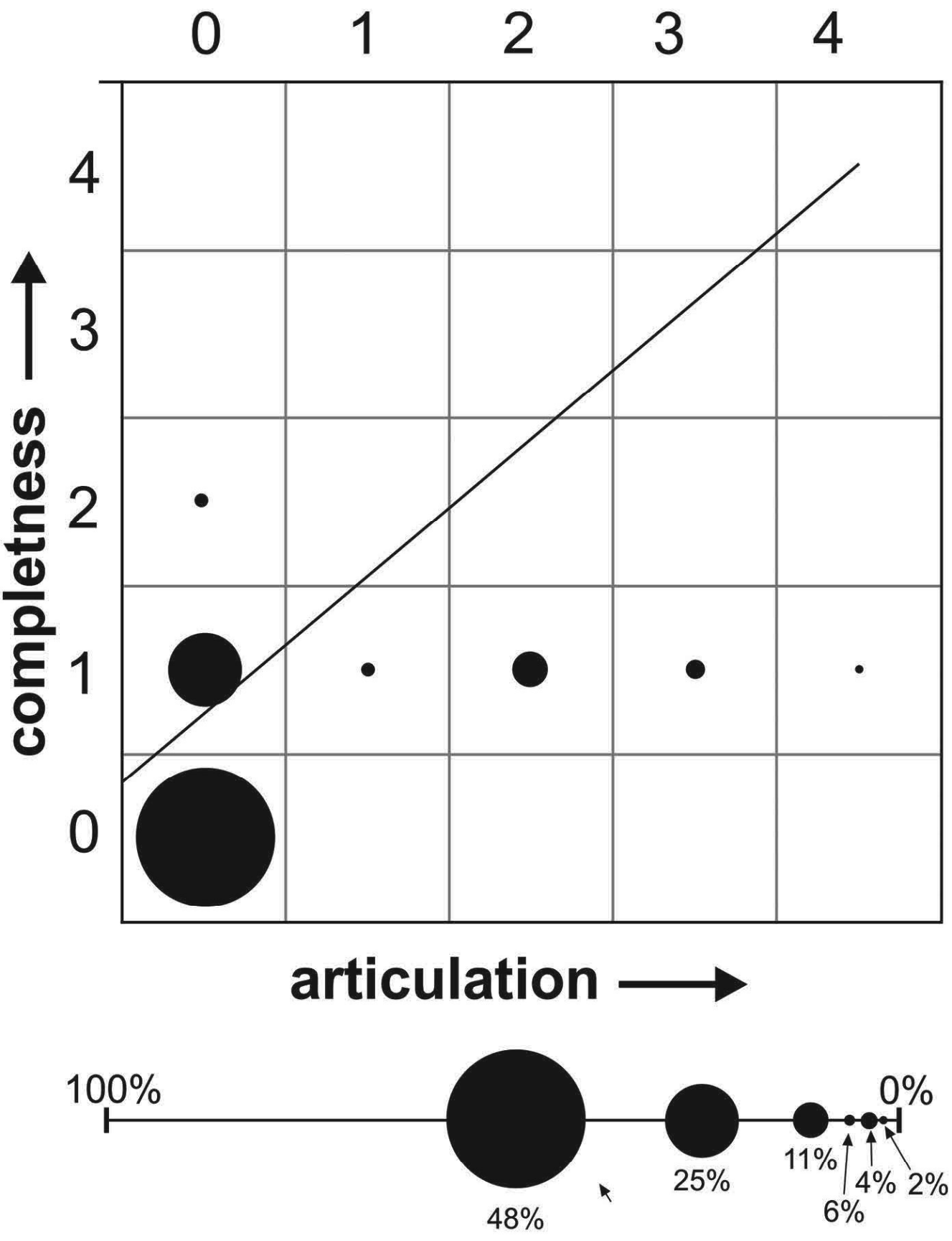
0
1
2
3
4
completness
articulation
100%
0%
48%
25%
11%
6%
4%
2%
r² = 1.38, rs = 0.47, T = 0.30

Figure 10

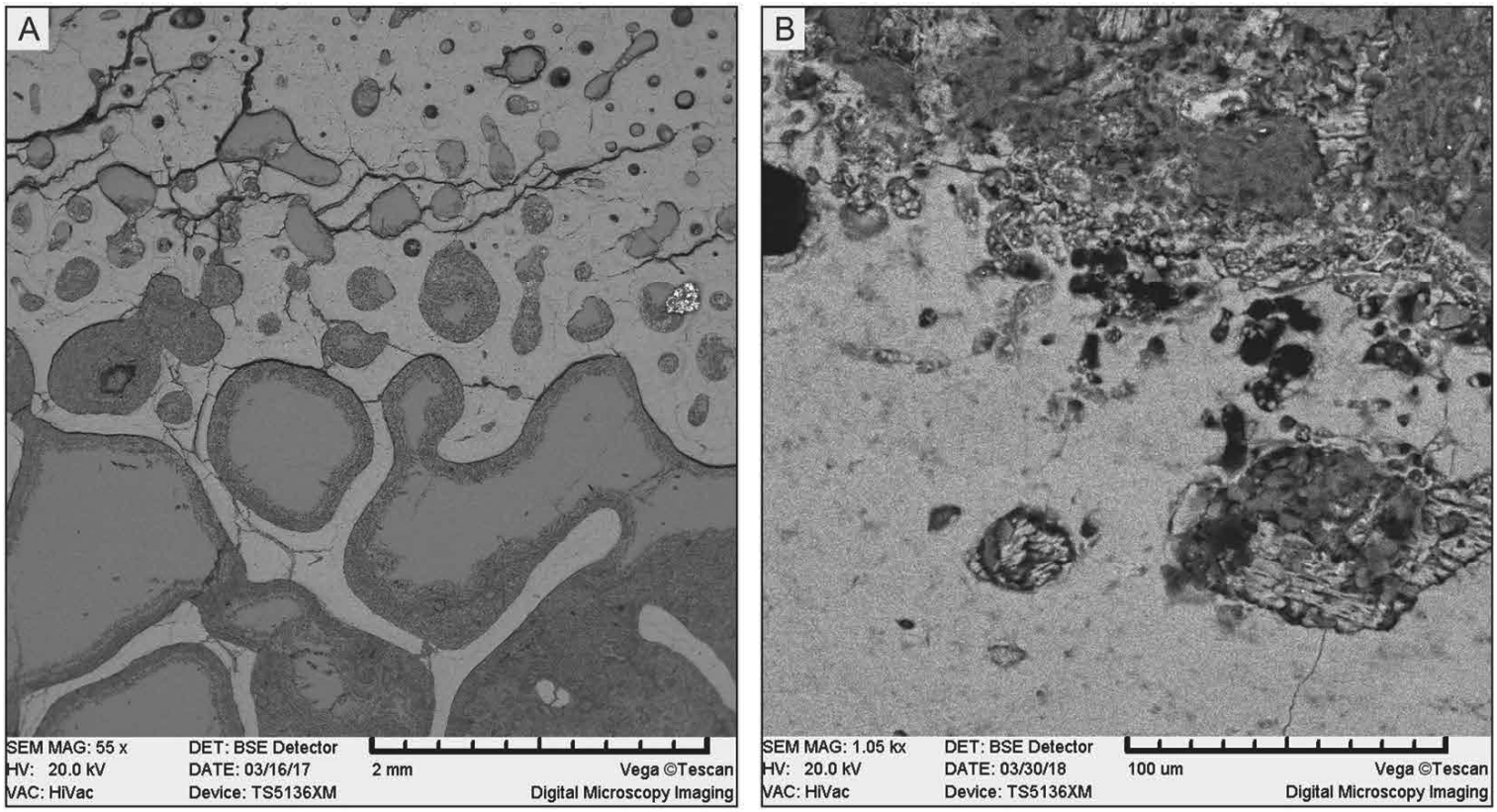
A
SEM MAG: 55 x
HV: 20.0 kV
VAC: HiVac
DET: BSE Detector
DATE: 03/16/17
Device: TS5136XM
2 mm
Vega ©Tescan
Digital Microscopy Imaging
B
SEM MAG: 1.05 kx
HV: 20.0 kV
VAC: HiVac
DET: BSE Detector
DATE: 03/30/18
Device: TS5136XM
100 um
Vega ©Tescan
Digital Microscopy Imaging
C
1 mm
D
500 µm
E
1 mm
F
100 µm

Figure 11

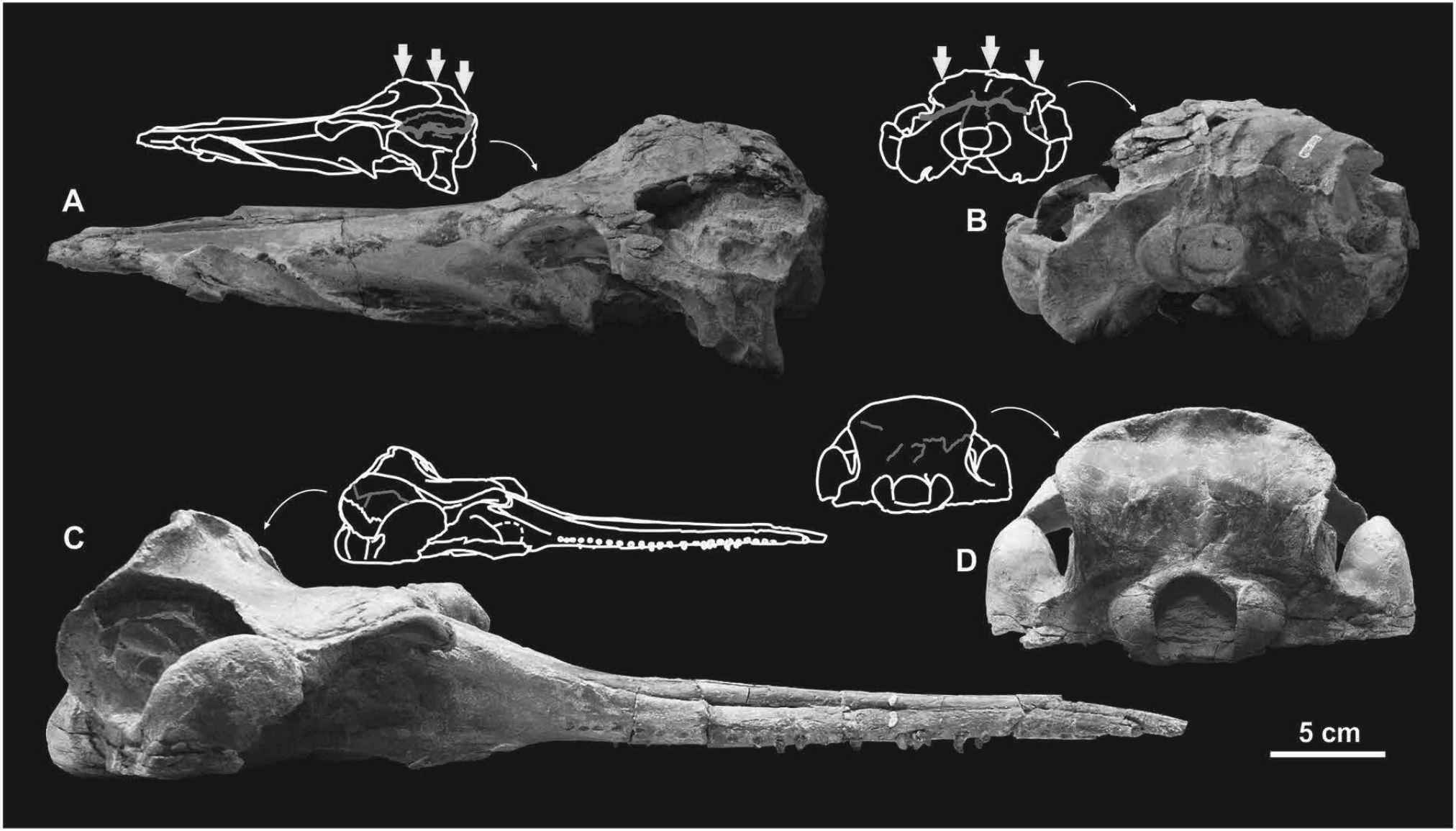

Figure 12

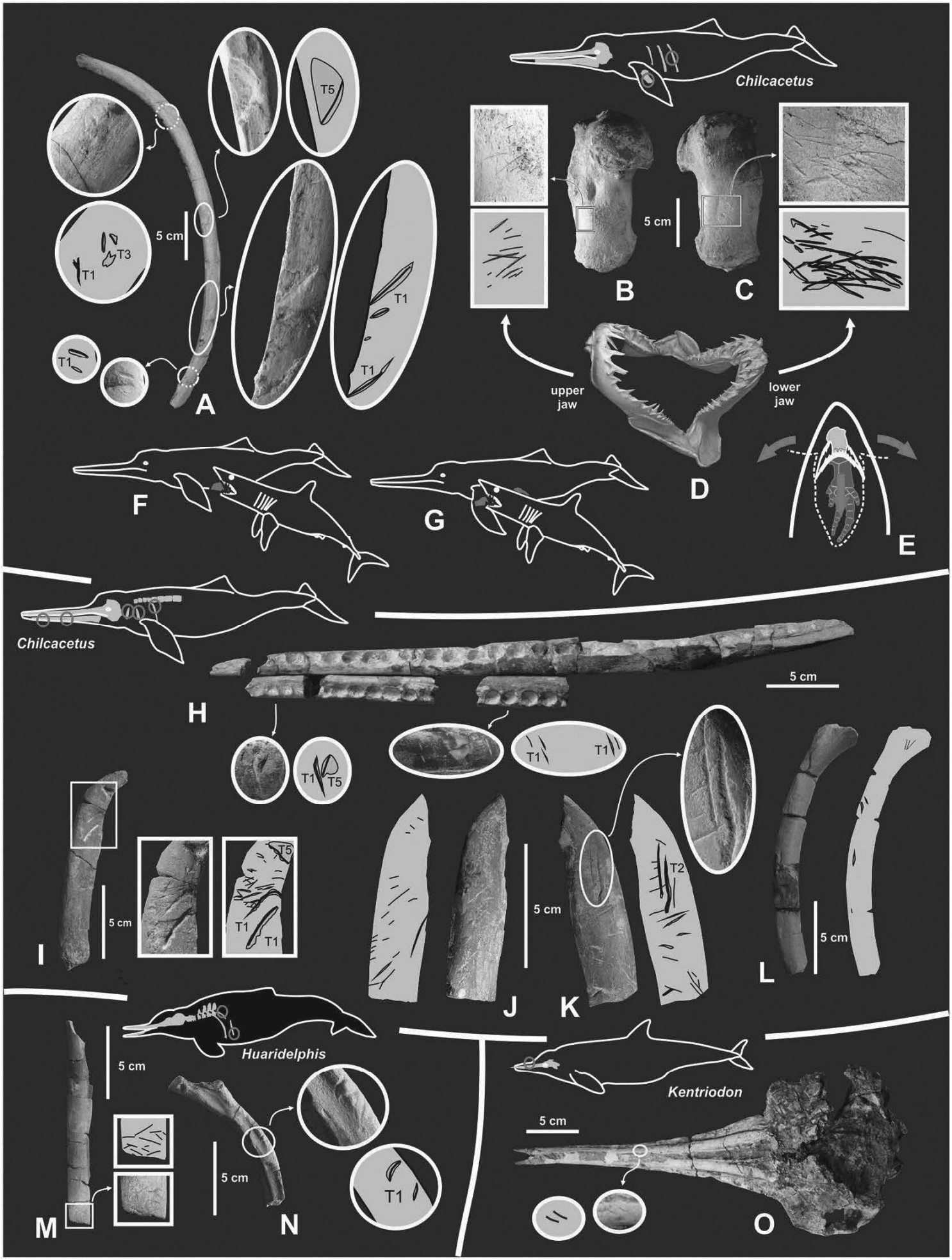
Chilcacetus
T5
T1
T3
5 cm
A
B
C
upper jaw
lower jaw
D
E
F
G
Chilcacetus
H
5 cm
T1
T5
I
T2
J
K
L
Huaridelphis
M
N
Kentriodon
O

Figure 13

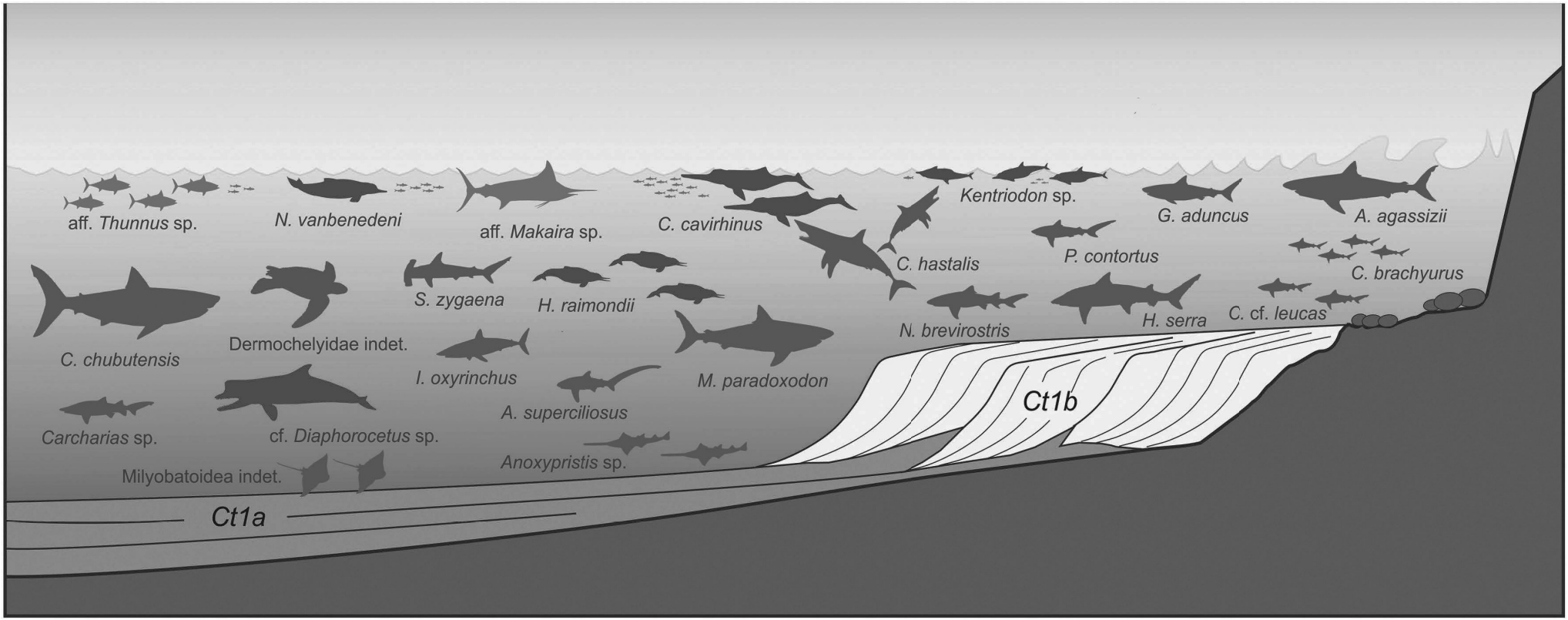
aff. Thunnus sp.
N. vanbenedeni
aff. Makaira sp.
C. cavirhinus
Kentriodon sp.
G. aduncus
A. agassizii
C. hastalis
P. contortus
C. brachyurus
S. zygaena
H. raimondii
C. chubutensis
Dermochelyidae indet.
N. brevirostris
H. serra
C. cf. leucas
I. oxyrinchus
M. paradoxodon
A. superciliosus
Ct1b
Carcharias sp.
cf. Diaphorocetus sp.
Anoxypristis sp.
Milyobatoidea indet.
Ct1a

Figure 14

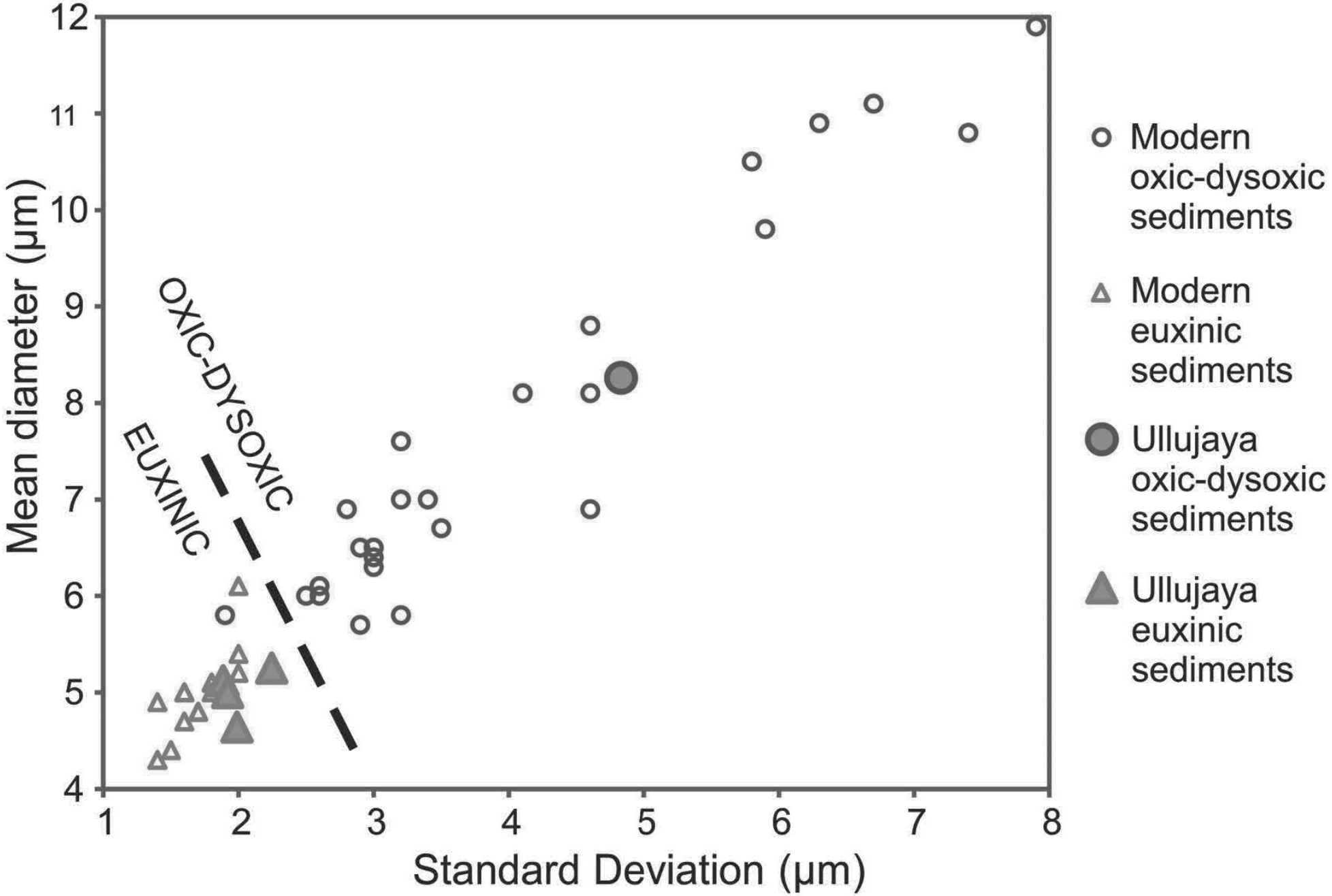
Mean diameter (µm)
Standard Deviation (µm)
OXIC-DYSOXIC
EUXINIC
Modern oxic-dysoxic sediments
Modern euxinic sediments
Ullujaya oxic-dysoxic sediments
Ullujaya euxinic sediments

Figure 15